https://doi.org/10.5194/egusphere-2026-2467
Preprint. Discussion started: 21 July 2026

Wide-swath satellite altimetry and novel subsurface temperature observations improve predictions in a dynamic western boundary current: System optimization and performance

Colette Kerry[1], Moninya Roughan[2], Shane Keating[1], and Gary B. Brassington[3,4]

[1]School of Mathematics and Statistics, UNSW Sydney Australia, Sydney, NSW, Australia 2052.
[2]Coastal and Regional Oceanography Lab, School of Biological, Earth and Environmental Sciences, UNSW Sydney Australia, Sydney, NSW, Australia 2052.
[3]Bureau of Meteorology, Sydney, Australia
[4]Now at Flowershift

Correspondence: Colette Kerry (c.kerry@unsw.edu.au)

Abstract.

Understanding and predicting regional and coastal ocean dynamics requires the effective combination of numerical models and observations that resolve key processes at suitable time and space scales. Fine-scale oceanic features and the ocean's complex subsurface structure remain a significant source of uncertainty in coastal and regional models due to lack of observations at necessary scales. Recently available observation platforms provide an unprecedented view of the ocean's fine-scale structure both at the surface (the Surface Water and Ocean Topography satellite mission, SWOT) and below the surface (using data from the Fishing Vessel Observation Network, FVON). Here we use advanced data assimilation to demonstrate the impact of these novel observation types on dynamic ocean state estimates in an eddy-dominated western boundary current region, the East Australian Current. First we show that these newly available observations benefit from an updated data assimilation configuration. Using this improved configuration, we show that the inclusion of SWOT data improves model representation of both the ocean surface across scales and of subsurface temperature (as observed by FVON). Assimilating FVON data, which drastically increases subsurface information in the coastal and shelf region, significantly improves subsurface temperature representation. Using novel observations from SWOT and FVON in a realistic ocean model, we show enhanced representation of ocean structure, particularly below the surface, essential for improved ocean forecasts and projections.

Keywords: East Australian Current (EAC), Four-Dimensional Variational (4D-Var) Data Assimilation, mesoscale, submesoscale, prediction, Western Boundary Current, ROMS, subsurface, SWOT, Fishing Vessels as Ships of Opportunity (FishSOOP), Fishing Vessel Observation Network (FVON), Observing System Experiments, OSEs

Key Points:

1. An updated data-assimilation configuration achieves improved fit to assimilated surface and subsurface observations and to independent in situ observations.

https://doi.org/10.5194/egusphere-2026-2467
Preprint. Discussion started: 21 July 2026

2. Inclusion of SWOT data improves model representation of sea surface height across scales, subsurface temperature in the coastal and shelf regions, and surface velocities.
3. Assimilation of FVON data significantly improves subsurface temperature representation in coastal and shelf regions.

1 Introduction

Accurate estimates of the past, present and future ocean states are crucial to effectively manage our ocean environment. Ocean state estimates require the combination of numerical models and ocean observations through data assimilation; observations are typically sparse in time and space or surface intensified (as viewed from satellites) and models allow us to place these observations in dynamical context (e.g. Moore et al., 2019). Ocean prediction at regional and coastal scales requires the effective combination of numerical models and observations that resolve key dynamical processes at suitable time and space scales (Jacobs et al., 2021; Edwards et al., 2024). A key knowledge gap exists around the representation of fine-scale flows (including submesoscales) in ocean models, due to the rapidly evolving flow and lack of observations at necessary scales. Likewise, the ocean's subsurface structure is often complex and remains typically undersampled making model estimates below the surface uncertain (Gwyther et al., 2022, 2023a, b). Data assimilation is particularly challenging in regions of complex circulation, such as eddy-rich oceanic regions and shelf seas, where the circulation contains a broad range of time and space scales (e.g. Walstad and McGillicuddy, 2000; Edwards et al., 2015, 2024).

The goal of any data assimilation scheme is to combine observations and a numerical model such that the result is a better estimate of the ocean circulation than either alone (e.g. Martin et al., 2024). Key to effective combination of the model and observations are prior assumptions around the uncertainty associated with each. Advanced data assimilation methods (e.g. 4-Dimensional Variational data assimilation (4D-Var) and the Ensemble Kálmán Filter (EnKF), Moore et al., 2020) make use of the time-variable dynamics of the model, allowing the observations to be assimilated over a time interval given the temporal evolution of the circulation. In 4D-Var (Moore et al., 2004) the model and observations are combined by minimising an objective cost function that measures normalised deviations of the modelled ocean state from the observations as well as from the modelled background state. The observation term of the cost function is given by the squared difference between the observations and the model, weighted by the inverse of the observation uncertainty covariance to prevent 'over-fitting' the solution to uncertain observations. The model background term is given by the squared model increment, weighted by the inverse of the background uncertainty covariance matrix, which carries the statistical information of the model prior and is key to accurately projecting the information contained by the observations onto the model state estimate. A key challenge associated with assimilation of temporally and spatially sparse observations in dynamically active regions relates to the specification of the background uncertainty covariances (Moore et al., 2019).

Effectively observing coastal and regional waters is particularly challenging given the scales of oceanic variability. Methods to assess the value of observations on model state estimates and analyses can inform observing strategies and advances in data assimilation approaches can optimize their value (Edwards et al., 2024). Studies in the East Australian Current (EAC) region using advanced data assimilation (4D-Var) provide a broad understanding of observation impact in this dynamic WBC region

https://doi.org/10.5194/egusphere-2026-2467
Preprint. Discussion started: 21 July 2026

(Kerry et al., 2018; Siripatana et al., 2020; Gwyther et al., 2022, 2023a; Kerry et al., 2025). They show that observations taken in regions with greater natural variability contribute most to constraining the model estimates, and subsurface observations have a high impact relative to the number of observations. Significantly, sampling the downstream eddy-rich region provides constraint to the upstream circulation, whereas observing the coherent jet upstream provides less value to estimates of the downstream eddy field. Kerry et al. (2020) highlight the challenges associated with predictability of fine-scale flows such as cyclonic eddies inshore of the EAC that are rapidly decorrelated from the initial state, noting that submesoscale predictability presents additional challenges to that of the more slowly-evolving mesoscale flows. Below the surface, complex structures require constraint from observations such as gliders (Siripatana et al., 2020), while in the absence of subsurface constraint structure below the surface can be degraded (Gwyther et al., 2022, 2023b, a). Likewise, assimilation of subsurface observations (e.g. data from gliders) requires assimilation in combination with surface observations to suppress unrealistic features and improve the impact of the subsurface observations (Pasmans et al., 2019). Assimilation of high-frequency in situ mooring observations improved representation of fine-scale variability in the California Current system as measured by independent glider and mooring observations, with the impacts dependent on the specific flow scenarios (Archer et al., 2022).

Recently available observation platforms provide an unprecedented view of the ocean's fine-scale structure both at the surface with the Surface Water and Ocean Topography satellite mission (SWOT) and below the surface with the Fishing Vessel Observation Network (FVON, known as Fishing Vessels as Ships of Opportunity Program - FishSOOP in Australia). The SWOT mission provides the first-ever synchronous 2D maps of sea surface height (SSH) at ∼2 km resolution, albeit at low temporal resolution (21-day repeat passes, Chelton, 2024; Morrow et al., 2019). FVON / FishSOOP has provided a step-change in the availability of subsurface temperature data (since 2022), providing high-resolution observations from sensors mounted on fishing equipment in coastal, shelf and open-ocean regions (Vranken et al., 2023; Jakoboski et al., 2024; Lago et al., 2025b).

Combining these newly available observations with a high-resolution model provides a unique opportunity to develop ocean state estimates that represent finer scale oceanic features. Initial attempts to assimilate SWOT data in a realistic submesoscale permitting model revealed the positive impact on both mesoscale and submesoscale representation (Kerry et al., 2026a). This study showed that assimilating SWOT data improves representation and prediction of the larger-scale mesoscale motions, consistent with results from Observing System Simulation Experiments (OSSEs) by Bonaduce et al. (2018); D'Addezio et al. (2019); Tchonang et al. (2021); Liu et al. (2024). Kerry et al. (2026a) also found that assimilation of SWOT data improves representation (but not prediction) of the fine-scale dynamics. Using OSSEs, Kerry et al. (2024a) demonstrated the value of assimilating FVON data on model representation of subsurface temperature, and show that the successful assimilation of these high-resolution subsurface observations requires careful configuration of the data assimilation system to optimize the way in which the observations inform the numerical model estimates. The potential value of FVON observations in informing complex subsurface structure in the EAC was highlighted in Lago et al. (2025b), and their positive impact on coastal forecasts around NZ was demonstrated by Azevedo Correia de Souza and de Godoi Rezende Costa (2026). Here we build on Kerry et al. (2026a) and Kerry et al. (2024a) to combine SWOT and FVON observations with a regional model of a dynamic western boundary current (WBC), the EAC, using comprehensively-used 4D-Var data assimilation infrastructure (Kerry et al., 2016, 2018, 2024b, 2025).

https://doi.org/10.5194/egusphere-2026-2467
Preprint. Discussion started: 21 July 2026

The EAC system exhibits dynamic eddying circulation that varies across a range of time and space scales, making it challenging to observe, model and predict. This dynamic region serves as an excellent platform for testing a data assimilating ocean model's capacity to capture fine-scale dynamics and complex subsurface structure. This study focuses on assessing the impact of SWOT and FVON data on predicting the surface and subsurface ocean circulation in the EAC region. We focus on a 1-year period (Aug 2023-Jul 2024) due to the concurrent availability of SWOT and FVON data as well as a unique set of independent observations (Figure 1, Section 2.3). These include high spatial resolution subsurface observations from a research cruise, glider observations, and drogued surface drifters providing high resolution surface velocity data. Combining a regional model of the EAC (Section 2.2) with observations using 4D-Var data assimilation (Section 2.4), we present a total of 6 data-assimilating numerical model experiments (Section 2.5, Table 1). The experiments vary in their data assimilation configuration and in the observations that they ingest: assimilating traditionally available data streams (satellite-derived Sea Surface Height and Sea Surface Temperature, and temperature and salinity from Argo profiling floats) alone or in concert with SWOT and/or FVON data.

First we present a strategy for optimization of the data assimilation configuration through adjustments to prior observation and model background uncertainty estimates (Section 2.6). We assess model performance using average statistics over the 1-year period that compare the model solutions with assimilated surface and subsurface observations and independent in situ observations (Section 3). We demonstrate that the updated configuration achieves an improved fit to assimilated and independent observations (Section 4). We then use the updated configuration to assess the impact of observations collected by SWOT and in situ observations collected through FVON, in addition to the traditionally assimilated data streams. We show that inclusion of SWOT data improves model representation of sea surface height across scales, subsurface temperature in the coastal and shelf regions, and surface velocities (Section 5). Assimilation of FVON data significantly improves subsurface temperature representation in coastal and shelf regions (Section 6).

https://doi.org/10.5194/egusphere-2026-2467
Preprint. Discussion started: 21 July 2026

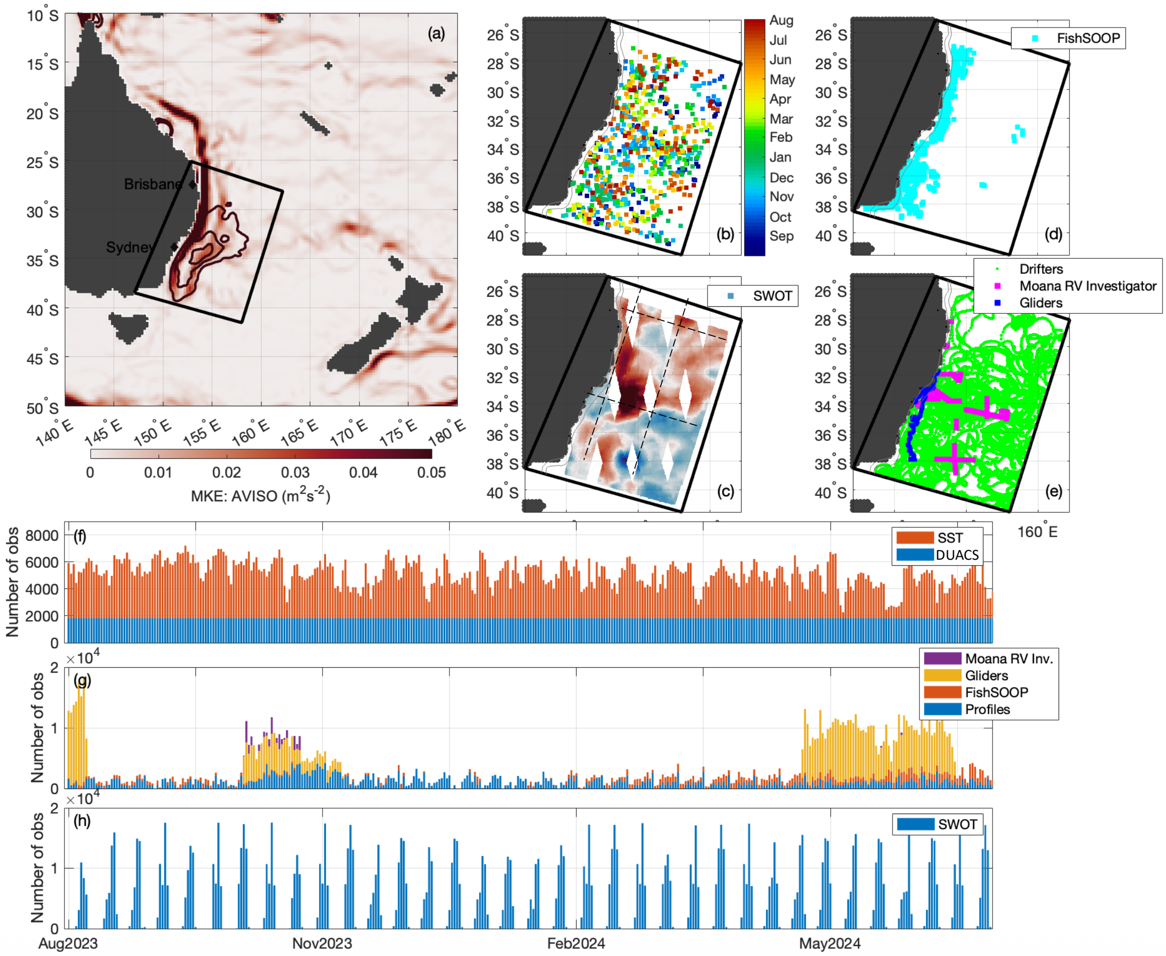

Figure 1. (a) Mean Kinetic Energy from DUACS, with mean Eddy Kinetic Energy contours, showing the circulation in the EAC system and the model domain (black box). (b) Location of assimilated Argo profile observations colour-coded by date. (c) Example of SWOT SSH coverage for a 6-day period (6-12 Oct 2023). (d) Location of assimilated FVON / FishSOOP observations. (e) Location of drifters, Moana sensors aboard the RV Investigator and glider observations used for independent verification. (f) Number of DUACS SSH and daily SST observations (after processing), (g) number of in situ observations (after processing), and (h) number of SWOT observations (after processing) per day.

2 Hydrodynamic Model and Data Assimilation System Configuration

The methodology described here expands on that used in Kerry et al. (2026a). This paper presents an updated data assimilation configuration and number of new experiments to elucidate the impact of SWOT and FVON observations, alone and in combination. While much of the model and data assimilation methodology described below was previously published in the

https://doi.org/10.5194/egusphere-2026-2467
Preprint. Discussion started: 21 July 2026

Supporting Information of Kerry et al. (2026a), it is necessary to repeat and build on this information for the purpose of this article.

2.1 Study Region

The EAC is the WBC of the South Pacific subtropical gyre (Figure 1a), advecting warm water along the southeastern coast of Australia (Oke et al., 2019). The position of the EAC jet and its associated eddies are responsible for the significant ocean variability experienced off southeastern Australia (Cetina Heredia et al., 2014; Sloyan et al., 2016; Kerry and Roughan, 2020) and the non-uniform warming trends (Malan et al., 2021). Along the extent of the EAC system, eddies can directly influence shelf circulation (Roughan et al., 2011; Schaeffer et al., 2014; Schaeffer and Roughan, 2015; Malan et al., 2023). When the current jet separates from the coast, large warm-core eddies are shed with cold-core eddies between them. These eddies propagate and evolve (Pilo et al., 2015a, b) and often exhibit complex vertical structure including tilting and stacking (Oke and Griffin, 2011; Macdonald et al., 2013; Roughan et al., 2017; Pilo et al., 2018; Rykova and Oke, 2022).

2.2 The Regional Ocean Modeling System Configuration

We use the Regional Ocean Modeling System (ROMS version 4.2) to simulate the ocean circulation off the southeastern coast of Australia between August 2023 - July 2024 as part of the South East Australian Coastal Ocean Forecast System (SEA-COFS, Roughan and Kerry, 2023)). ROMS is a widely used free-surface, hydrostatic, terrain-following, primitive equation ocean model and is described by Haidvogel et al. (2000); Shchepetkin and McWilliams (2005). The model configuration used in this study has been used for a decade of research in the EAC System and is described in detail in Kerry et al. (2016, 2020); Roughan and Kerry (2023); Kerry et al. (2026a).

The study domain covers the latitudinal extent of the EAC system including the five core dynamical regimes from where the current jet is most coherent, the EAC separation region, the EAC retroflection, the region of high eddy activity associated with the EAC eastern extension, and the EAC southern extension (Oke et al., 2019, , Figure 1a). The model has a varying cross-shore horizontal resolution, increasing from 2.5 km over the continental shelf to 6 km offshore, and a 5 km horizontal resolution in the along-shore direction. Higher resolution over the shelf allows the steep topography to be maintained while minimizing pressure gradient errors that emerge in terrain-following coordinate schemes (Haney, 1991; Mellor et al., 1994). In the vertical, we use 30 s-layers with the vertical stretching scheme of De Souza et al. (2015) applied.

Initial conditions and boundary forcing are derived from the Bureau of Meteorology (BOM) OceanMAPS forecast (Brassington et al., 2023), similarly to earlier configurations (Kerry et al., 2026a). The model is forced at the surface with realistic atmospheric forcing derived from BOM's ACCESS-R atmospheric forecast.

A longterm free-running configuration accurately represents the mean dynamical features of the EAC and its variability, both at the surface and at depth (Kerry and Roughan, 2020; Li et al., 2021, 2022). Specifically, these studies show that the model accurately represents the mesoscale eddy related variability in SSH, the latitudinal distribution of EAC separation, the seasonal cycle in sea surface temperature (SST), the ocean's general subsurface structure based on data from Argo profiling floats, EAC transport and the temperature depth structure across the EAC.

https://doi.org/10.5194/egusphere-2026-2467
Preprint. Discussion started: 21 July 2026

2.3 Observations

Here we combine the EAC-ROMS hydrodynamic model with observations (Section 2.3) using 4D-Var data assimilation (Section 2.4) over a 1-year period (August 2023 - July 2024). The assimilated observations include a combination of the observations described in Sections 2.3.1-2.3.5 (refer to Table 1). Model experiments are compared to all observations, including observations that are independent to all experiments (Section 2.3.6). The number of processed observations per day is shown in Figure 1f,g,h.

2.3.1 Nadir altimeter derived Sea Surface Height

Along-track satellite altimetry data are merged to produce a global, daily, gridded (1/4° x 1/4°) mean sea level anomaly (SLA) product, computed with respect to a seven-year mean, using the Data Unification and Altimeter Combination System (DUACS). We use the level-4 gridded Near Real Time (NRT) product CMS (2024) which is produced for operations, delivered every day and uses a non-centered processing time-window with a 6-day delay (as future data is not available). We add the AVISO SLA data to the dynamic Sea Surface Height (SSH) mean from a longterm free running model such that the sea level data is consistent with the ROMS model configuration (a standard procedure shown to be effective in numerous studies, e.g., Moore et al., 2011a; Matthews et al., 2012a; De Souza et al., 2015; Kerry et al., 2016; Wilkin et al., 2022). As the DUACS gridded product poorly resolves continental shelf processes, we exclude SSH observations over water depths less than 1000 m.

2.3.2 Satellite-derived Sea Surface Temperature

Four different satellite-derived Sea Surface Temperature (SST) products are used for this study (VIIRS, VIIRS2, NAVO and AMSR2). For assimilation, we average all SST data to a grid of $\sim$ 15 km resolution (approximately 3 model grid cells by 3 model grid cells) and to daily intervals, and assimilate the data at midnight every day. This data thinning approach is employed such that the number of SST observations is of similar order of magnitude to the number of SSH observations (Figure 1f), ensuring that SST does not overly dominate the cost function (e.g. Kerry et al., 2016). SST data is removed inside the 300 m bathymetry contour.

2.3.3 Argo floats (Temperature and Salinity Profiles)

Argo (free-drifting profiling) floats measure pressure, temperature and salinity of the upper 2000 m of the global ocean (www.argo.ucsd.edu, Figure 1b). The Argo data points are averaged to the model grid (in the horizontal and vertical) and a 5-minute time-step. Following Wilkin et al. (2022), we repeat the profiles every 2 hours within a two-day time interval (at actual time $\pm$1 day).

2.3.4 Surface Water and Ocean Topography Sea Surface Height observations

The SWOT mission uses both a nadir altimeter and a Ka-band Radar Interferometer (KaRIN) to measure ocean surface topography. SWOT measurements are at a nominal resolution of 2 km over a 130 km wide swath with near-global spatial coverage

https://doi.org/10.5194/egusphere-2026-2467
Preprint. Discussion started: 21 July 2026

every 21 days. Here we use the noiseless SSH anomaly (SSHA) from the Level 3 v102 expert data (AVISO/DUACS, 2024; Tréboutte et al., 2023; Dibarboure et al., 2025). As with the gridded DUACS data (Section 2.3.1), we add the SWOT SLA data to the dynamic SSH mean from a longterm free running model for assimilation. Six-day windows allow for several swath passes to be assimilated in each window (e.g. Figure 1c). Unlike DUACS SSH observations, SWOT data is not excluded over shallow water depths.

2.3.5 Fishing Vessels as Ships of Opportunity (FishSOOP) subsurface temperature observations

Australia's Fishing Vessel Observation Network (FVON, known as FishSOOP in Australia) is a collaborative project between research and industry, initially co-funded by the Fisheries Research and Development Corporation (FRDC) and Australia's Integrated Marine Observing System (IMOS), to install temperature sensors on commercial fishing vessels around Australia (Lago et al., 2025b). FishSOOP is a founding partner of the International Fishing Vessel Observation Network (FVON). Low-cost research-quality temperature sensors (Zebratech Moana TD 200 m, 1000 m, or 2000 m sensors) are installed on the fishing equipment and collect data during routine fishing operations. The collaborative data collection has provided a step-change in the availability of in-situ temperature observations, primarily on and near the continental shelf (Figure 1c, Figure 6). Data are processed using IMOS standards and quality control flags applied as per Lago et al. (2025a). The FVON observations will be hereafter referred to as FishSOOP in this paper.

2.3.6 Independent Observations used for system assessment

A suite of additional observations were also available over the data rich simulation period. These data are independent observations against which we assess the performance of the model experiments.

A 3-week research cruise aboard Australia's Marine National Facility, the RV Investigator, was completed in Oct. 2023. The cruise provides detailed 3-dimensional observations of oceanic eddies and fronts in the EAC (Azaneu et al., 2026), delivering a unique opportunity to comprehensively validate our subsurface ocean state estimates. Here we make use of data from additional Moana temperature sensors that were deployed on equipment during the research cruise (Figure 1e,h).

Temperature and salinity data from ocean gliders, operated through IMOS, was available in Aug. 2023, Oct. 2023 and May-June 2024 (Figure 1e,g). Gliders are intended to routinely measure across the continental shelf along the inside edge of the EAC (e.g as per Schaeffer et al., 2015), with some missions extending off the shelf before recovery.

Twenty-six Surface Velocity Program drifters (SVPs) from the Global Drifter Program (GDP; Elipot et al., 2016) entered the model domain between August 2023 and July 2024 (Figure 1e), including 19 deployed during the 2023 research voyage (Matisons et al., 2026). SVP drifters are satellite-tracked buoys drogued at 15 m depth that measure surface current velocities, which are interpolated to six-hourly intervals in the GDP dataset. Drifter quality control follows the method described in Elipot et al. (2016). Surface velocities are low-pass filtered using a second-order Butterworth filter with a 25 hour cut-off to remove tidal and inertial oscillations (as in Tranchant et al., 2025).

https://doi.org/10.5194/egusphere-2026-2467
Preprint. Discussion started: 21 July 2026

2.4 Data Assimilation Methodology

A description of the classic state estimation problem and how it is applied in 4D-Var is outlined in Kerry et al. (2024b). A detailed description of the ROMS 4D-Var formulation and implementation is described by Moore et al. (2011c, a, b), and it has been used successfully in many applications (e.g. Di Lorenzo et al., 2007; Powell et al., 2008; Powell and Moore, 2008; Broquet et al., 2009; Matthews et al., 2012b; Zavala-Garay et al., 2012; Janeković et al., 2013; Souza et al., 2014; Kerry et al., 2016; Gwyther et al., 2022; Wilkin et al., 2022).

4D-Var uses variational calculus to solve for increments in model initial conditions, boundary conditions, and forcing such that the differences between the observations and the new model trajectory (described by a cost function) is miminized – in a least-squares sense – over a specific assimilation window. The goal is for the model to represent all of the observations in time and space using the physics of the model, and accounting for the uncertainties in the observations and background model state, producing a description of the ocean state that is dynamically balanced and a complete solution of the nonlinear model equations. As such, key components of a 4D-Var system are prior estimates of the background (prior model) uncertainties (**P**) and the observation uncertainties (**R**), which are important scaling factors in the cost function. The formulation of the cost function and the background error covariance matrix is described in detail in Kerry et al. (2016, 2024b).

The background uncertainty covariance matrix should represent the expected uncertainties in the model and is estimated here by factorization (Weaver and Courtier, 2001). In classic 4D-Var (used here) the background uncertainty covariance matrix is based on information about the dominant dynamical balances of the system, as well as the average statistics of errors in the forecast system (Lorenc, 2003). The covariances are assumed to be static with isotropic horizontal and vertical length scales (refer to Kerry et al., 2026a); flow-dependence is introduced through the tangent-linear and adjoint models. In practice, formulation of the background uncertainty covariance matrix requires prior estimates of the uncertainty associated with the background model (standard deviations of the model fields taken from a long-term model simulation) and estimates of the characteristic horizontal and vertical decorrelation length scales. The observation uncertainties should represent both the instrument error and errors of representativeness, which account for unresolved processes and scales in the model (Oke and Sakov, 2008).

The specific prescribed prior observation and background uncertainties for the model experiments used in this study are described in Section 2.6.1, 2.6.2 and Table 1. To attempt to optimize the system, an iterative approach was used in the specification of the prior choices of observation uncertainties (**R**) and the standard deviations and length scales used to compute (**P**). This approach is presented in Section 2.6.

2.5 Model Experiments

We use the EAC-ROMS data assimilating model configuration used in Kerry et al. (2026a) and previously described in Kerry et al. (2016, 2018, 2020). As with Kerry et al. (2026a), the model was configured over Aug 2023 - Jul 2024 and used an updated ROMS 4D-Var algorithm (the Restricted B-preconditioned Lanczos). Here we describe 6 4D-Var experiments (refer to Table 1), 3 of which were introduced in Kerry et al. (2026a); HotStart, TRAD and TRAD+SWOT. In all experiments, we adjust the

https://doi.org/10.5194/egusphere-2026-2467
Preprint. Discussion started: 21 July 2026

model initial conditions only (boundary and surface forcing are not included in the control vector) such that the new model solution (the analysis) better represents the observations over the assimilation interval. The analysis then provides the initial conditions for the subsequent forecast (model background estimate).

The TRAD experiment assimilates the 'traditionally available' observations; gridded SSH derived from along-track Nadir satellite altimetry data (Section 2.3.1), satellite-derived SST (Section 2.3.2) and temperature and salinity profiles from Argo floats (Section 2.3.3). The TRAD+SWOT experiment assimilates these 'traditionally available' observations in concert with the SWOT observations (Section 2.3.4). TRAD and TRAD+SWOT are identical to the experiments presented in Kerry et al. (2026a). As detailed in Kerry et al. (2026a) and Sections 2.6.1 and 2.6.2 below, the prior observation uncertainties applied to the DUACS SSH observations are inflated for TRAD+SWOT compared to TRAD, and the horizontal decorrelation length scales for SSH, u and v are reduced (Table 2.5.1). TRADshortTS and TRAD+SWOTsh assimilate the same observations as TRAD and TRAD+SWOT respectively, but have different (optimized) prior specified observation and background uncertainty estimates. This was achieved through an informed iterative process described in detail in Section 2.6. TRAD+FishSOOP and TRAD+SWOT+FishSOOP use the optimized prior uncertainties as in TRADshortTS and TRAD+SWOTsh, but also include the FishSOOP high resolution sub-surface temperature data.

The experiments are summarized in Table 1, which shows the observations that are assimilated in each experiment and the prior choices of observation uncertainties, horizontal and vertical decorrelation length scales and standard deviations (used in the calculation of the background error covariance matrix, Section ??). These are the tunable prior choices for the classic 4D-Var data-assimilation configuration in ROMS. We also compare the 4D-Var systems to a 'Hot Start' model run: here the ROMS free running model is initialized with OceanMaps every 6 days and no data assimilation is performed on the nested ROMS grid. The 'Free Run' (not included in Table 1) is initialized with OceanMaps at the initial time and integrated over the 1-year period without data assimilation. Comparisons to the Free Run (e.g. Table 3) are useful as a baseline to show the value of data assimilation.

2.5.1 Assimilation Configuration

In this study, we use a 6-day window so that the tangent linear assumption remains reasonably valid at this model resolution, and allowing a reasonable coverage of SWOT data for most 6-day periods. Previous work in the EAC (Kerry et al., 2016) and the Philippine Sea/Kuroshio region (for a ROMS model of similar resolution, Kerry and Powell, 2022) showed that the tangent linear assumption remains reasonably valid for realistic perturbations over 5-7 days in these dynamic regions. We find that 14 *inner* loops and a single *outer* loop give an acceptable reduction in the cost function (rather than a true minimum).

2.6 Prior Uncertainty Estimates: Consistency and Optimization

The validity of the prior assumptions of the background and observation uncertainties (Section 2.6.1 and 2.6.2) is important in determining the optimality of the analysis. Our goal is to generate a new time-varying ocean state estimate that is a complete solution of the ocean model equations and better fits the observations, taking into account the uncertainties of both the model background state (the initial estimate, or the forecast) and the observations. If the observation uncertainty is too large compared

https://doi.org/10.5194/egusphere-2026-2467
Preprint. Discussion started: 21 July 2026

Table 1. Model experiment details. For the observation platforms we show whether the observation platform is assimilated or not and the prescribed prior observation uncertainties. Standard deviations and decorrelation length scales refer to those used in the formulation of **P** (refer to, Kerry et al., 2024b).

Model experiment:	Hot Start	TRAD	TRAD+ SWOT	TRADshortTS	TRAD+ FISHSOOP	TRAD+SWOTsh	TRAD+SWOT +FISHSOOP
Window length	6 days	6 days	6 days	6 days	6 days	6 days	6days
Initial conditions	Ocean Maps	Previous analysis	Previous analysis	Previous analysis	Previous analysis	Previous analysis	Previous analysis
Assimilated observations							
DUACS SSH (prior uncertainty)	×	✓(6cm)	✓(8cm)	✓(6cm)	✓(6cm)	✓(6cm)	✓(6cm)
SWOT SSH (prior uncertainty)	×	×	✓(2-4cm)	×	×	✓(3-4cm)	✓(3-4 cm)
Midnight SST (prior uncertainty)	×	✓(0.4^{o}C)	✓(0.4^{o}C)	✓(0.4^{o}C)	✓(0.4^{o}C)	✓(0.4^{o}C)	✓(0.4^{o}C)
Argo temperature (prior uncertainty)	×	✓ (0.05-0.4^{o}C)	✓ (0.05-0.4^{o}C)	✓ (0.05-0.4^{o}C)	✓ (0.05-0.4^{o}C)	✓ (0.05-0.4^{o}C)	✓ (0.05-0.4^{o}C)
Argo salinity (prior uncertainty)	×	✓ (0.005-0.04)	✓ (0.005-0.04)	✓ (0.005-0.04)	✓ (0.005-0.04)	✓ (0.005-0.04)	✓ (0.005-0.04)
FishSOOP temperature (prior uncertainty)	×	×	×	×	✓ (QC1 and QC2, 0.05-0.4^{o}C) (QC3, 0.1-0.8^{o}C)	×	✓ (QC1 and QC2, 0.05-0.4^{o}C) (QC3, (0.1-0.8^{o}C)
Horizontal decorrelation scale (km)	N/A	100km	40km (SSH) 50km (u,v) 100km (T,S)	100km (SSH) 100km (u,v) 40km (T,S)	100km (SSH) 100km (u,v) 40km (T,S)	40km (SSH) 40km (u,v) 40km (T,S)	40km (SSH) 40km (u,v) 40km (T,S)
Vertical decorrelation scale (m)	N/A	30m	30m	30m	30m	30m	30m
Standard deviations	N/A	6-day doubled	6-day doubled	6-day tripled (doubled temp.)	6-day tripled (doubled temp.)	6-day tripled (doubled temp.)	6-day tripled (doubled temp.)

https://doi.org/10.5194/egusphere-2026-2467
Preprint. Discussion started: 21 July 2026

to the background the analysis will ignore the observation. If the observation uncertainty is too small, the analysis will over-fit to the observation and may develop an unphysical response. A measure of the consistency of the assimilation system given the prior uncertainty assumptions can be made using a set of diagnostics based on the innovation statistics, presented in Desroziers et al. (2005). These diagnostics are based on the observation minus background, observation minus analysis, and analysis minus background differences and provide a check of the consistency of the prior choices of the background and observation uncertainty covariances. The level of agreement between the a priori specified uncertainties (**B** and **R**), and the errors diagnosed a posteriori following the methods introduced by Desroziers et al. (2005) (hereafter referred to as the diagnostic errors) provides a measure of the appropriateness of the estimates of **B** and **R**.

Our prior observation uncertainty estimates were based on instrument accuracy and previous experience (for representation error), and our initial background uncertainty hypotheses related to mesoscale variability of the free-running model (as in Kerry et al., 2016). Then an iterative approach was used to adjust prior choices of both the observation and background uncertainties to improve the optimality of the analyses. For the ratios of diagnostic errors and prior observation and background uncertainties, a value of unity represents optimal consistency between the prior uncertainty choices and the diagnostic errors. Where the ratios of diagnostic errors to prior uncertainties are >1, prior specified uncertainty is less than optimal (over-fitting), and ratios <1 represent under-fitting. As seen in Table 2, the ratios for TRAD and TRAD+SWOT suggest there is some overfitting, while the adjustments made for the other 4 experiments achieve ratios closer to 1. Overall, updating the configurations such that they are closer to optimal (as described in Sections 2.6.1 and 2.6.2) translates to improved fit to assimilated and independent observations (Section 4).

2.6.1 Prior Observation Uncertainties

The prescribed observation uncertainties for the experiments presented in this study are given in Table 1. The DUACS delayed-time global SLA product error for the region is estimated at 2 cm (CMS, 2024). We prescribe an observation uncertainty of 6-8 cm to account for imbalances between this statistical field and a dynamically-balanced SSH field required by the model, and the higher spatial-scale processes resolved by the model compared to the gridded product.

For TRAD+SWOT (Kerry et al., 2026a), where SWOT is assimilated in concert with the conventional-altimeter-derived gridded DUACS product, the DUACS uncertainties were inflated from 6 cm to 8 cm. The reasoning was to allow the DUACS SSH to provide constraint when and where SWOT was not available, but to allow a tighter fit to the fine-scales resolved by SWOT when the SWOT observations were available. However, error diagnostics to check consistency of the prior observation and background uncertainty choices found that 6 cm was more appropriate for the DUACS observation uncertainty across all experiments (even with the inclusion of SWOT, Table 2).

The SWOT data (Level 3 v102 expert noiseless SSHA used here, AVISO/DUACS, 2024; Tréboutte et al., 2023; Dibarboure et al., 2025) has various corrections applied including removing tidal signals. The total SSH signal of processes that are observed by SWOT and that may not be effectively removed from the data (such as non-stationary internal tides) must be accounted for in the specified uncertainty. We prescribe observation uncertainties for SWOT of 2-4 cm for TRAD+SWOT (Kerry et al., 2026a), scaled linearly from 2 cm at the centre to 4 cm at the outer edge of the swath. For TRAD+SWOT both

https://doi.org/10.5194/egusphere-2026-2467
Preprint. Discussion started: 21 July 2026

the diagnosed observation and background errors are about two times bigger than the prior uncertainties, indicating overfitting (Table 2, Figure 2: top panels). We find that increasing the observation uncertainties slightly to 3-4 cm across the swath, and adjusting the background uncertainties (Table 2.5.1 and Section 2.6.2) resulted in across-swath ratios very close to unity for TRAD+SWOTsh (Figure 2) and TRAD+SWOT+FishSOOP (not shown).

For SST, the prescribed observation uncertainty is chosen to be the maximum of the variance of all observations that fall within an $\sim$ 15 km cell within the daily period (Section 2.3.2), and the specified product error which is 0.4 °C. The Argo data points are averaged to the model grid (in the horizontal and vertical) and a 5-minute time-step (Section 2.3.3). Uncertainty profiles are defined to specify the nominal minimal uncertainties for subsurface temperature and salinity (method and error profile shape presented in Kerry et al., 2016). The profiles provide greater uncertainties in the depth ranges of greatest variability, where representation errors are likely to be the largest. For temperature, the profiles have a value of 0.4 ^oC from the surface to $\sim$250 m depth (the region of greatest variability). Below 1000 m the value is set to 0.05 ^oC. The observation error variance is specified as the maximum of this nominal minimum error variance and the variance of the observations from the same model cell.

For the FishSOOP data, the nominal minimum uncertainty profiles are dependent on the prescribed quality control flags (Lago et al., 2025a). Quality control flags are applied to the FishSOOP data in line with IMOS protocol, with additional QC flags applied to the data location (to account for uncertainty of the location of the fishing equipment relative to the vessel, from which the location information is sourced). The flags refer to uncertainty on location <5 km (QC==1), 5-50km (QC==2), and uncertainty on location of >50km (QC==3). The latter is most common on long-line fishing vessels where the equipment can be a considerable distance from the vessel which records the position. For observations with quality control flags equal to 1 or 2, the same nominal minimum uncertainty profiles as Argo are used. For FishSOOP observations with quality control flags of 3, the nominal minimum uncertainty profiles are doubled to account for location uncertainty. As with Argo, FishSOOP data points are averaged to the model grid (in the horizontal and vertical) and a 5-minute time-step (Section 2.3.5), and the observation error variance is specified as the maximum of the nominal minimum error variance and the variance of the observations from the same model cell and time-step.

2.6.2 Prior Model Background Uncertainties

The model standard deviations and the horizontal and vertical decorrelation length scales used to formulate the background error covariance matrix are given in Table 1. The choice of length scales used for TRAD was comprehensively justified in Kerry et al. (2016) based on the goal of representing the mesoscale eddy field. In Kerry et al. (2026a), horizontal length scales for SSH and velocities were reduced when assimilating SWOT data (TRAD+SWOT) due to the resolution of finer-scale features by SWOT. To assess the sensitivity of the choice of horizontal length scales, Kerry et al. (2026a) performed an experiment with SWOT data that used the same length scales as TRAD, and showed that the shorter length scales used in TRAD+SWOT gave an improved fit to SWOT SSH observations across all scales and all sections, supporting the choice of reduced length scales.

Shorter length scales for temperature and salinity were also applied for TRADshortTS, TRAD+FISHSOOP, TRAD+SWOTsh and TRAD+SWOT+FishSOOP. This approach was taken because of the new availability of FishSOOP data which can measure

https://doi.org/10.5194/egusphere-2026-2467
Preprint. Discussion started: 21 July 2026

across fine-scale features, in constrast to previous experiments that assimilated only surface observations and in situ profiles from Argo floats. The choice of shorter decorrelation length scales for the background error covariance matrix was also based on results from Kerry et al. (2024a) that showed that shorter length scales prevent overfitting to localised observations and improve model-observation agreement away from the fishing vessel mounted observations.

Sensitivity analysis was performed on the vertical length scales (10 m, 30 m, 50 m and 100 m). A vertical decorrelation length scale of 30 m was found to be optimal to represent the complex vertical structure in the observed profiles while preventing unrealistic vertical structure in the profile adjustments.

The standard deviations were initially computed as the square root of the mean 6-day variances from a long (6.5 year, 2012-2019) free-running simulation. Guided by a posteriori analysis of the initial simulations (following Desroziers et al., 2005, refer to Section 2.6), the standard deviations were doubled for TRAD and TRAD+SWOT to provide more consistent background error estimates. For TRADshortTS, TRAD+FishSOOP, TRAD+SWOTsh and TRAD+SWOT+FishSOOP, the standard deviations for temperature were doubled (as in TRAD and TRAD+SWOT) and standard deviations for all other variables were tripled, effectively relaxing the fit to the model background.

Table 2. Ratio of diagnostic errors and prior uncertainties for observations and mode background as per Desroziers' equations (Desroziers et al., 2005). Values are given for the model domain and averaged over the one-year period. The ratio for observations is outside of brackets and the ratio for model background is in brackets. For the ratios of diagnostic errors and prior uncertainties, a value of unity represents optimal consistency between the prior uncertainty choices and the diagnostic errors. Where the ratios of diagnostic errors to prior observation (background) uncertainties are >1, prior specified observation (background) uncertainty is less than optimal (over-fitting). Ratios <1 represent under-fitting.

Model experiment:	TRAD	TRAD+ SWOT	TRADshortTS	TRAD+ FISHSOOP	TRAD+SWOTsh	TRAD+SWOT +FISHSOOP
DUACS SSH	1.54 (1.17)	0.93 (1.27)	0.94 (0.69)	1.08 (0.73)	0.83 (0.69)	0.92 (0.74)
SWOT SSH	N/A (N/A)	1.70 (1.94))	N/A (N/A)	N/A (N/A)	1.01 (1.00)	1.1 (1.06)
Midnight SST	1.23 (0.91)	1.22 (0.96)	0.59 (0.55)	0.62 (0.57)	0.61 (0.54)	0.63 (0.54)
Argo Subsurface Temp.	1.24 (1.39)	1.25 (1.39)	0.81 (1.13)	0.93 (1.17)	0.86 (1.11)	0.89 (1.10)
Argo Subsurface Salinity	1.26 (1.79)	1.41 (1.80)	0.93 (1.11)	1.00 (1.16)	1.02 (1.08)	1.13 (1.03)
FishSOOP Subsurface Temp. QC1+2	N/A (N/A)	N/A (N/A)	N/A (N/A)	1.05 (0.76)	N/A (N/A)	1.13 (0.73)
FishSOOP Subsurface Temp. QC3	N/A (N/A)	N/A (N/A)	N/A (N/A)	0.43 (0.45)	N/A (N/A)	0.44 (0.50)

https://doi.org/10.5194/egusphere-2026-2467
Preprint. Discussion started: 21 July 2026

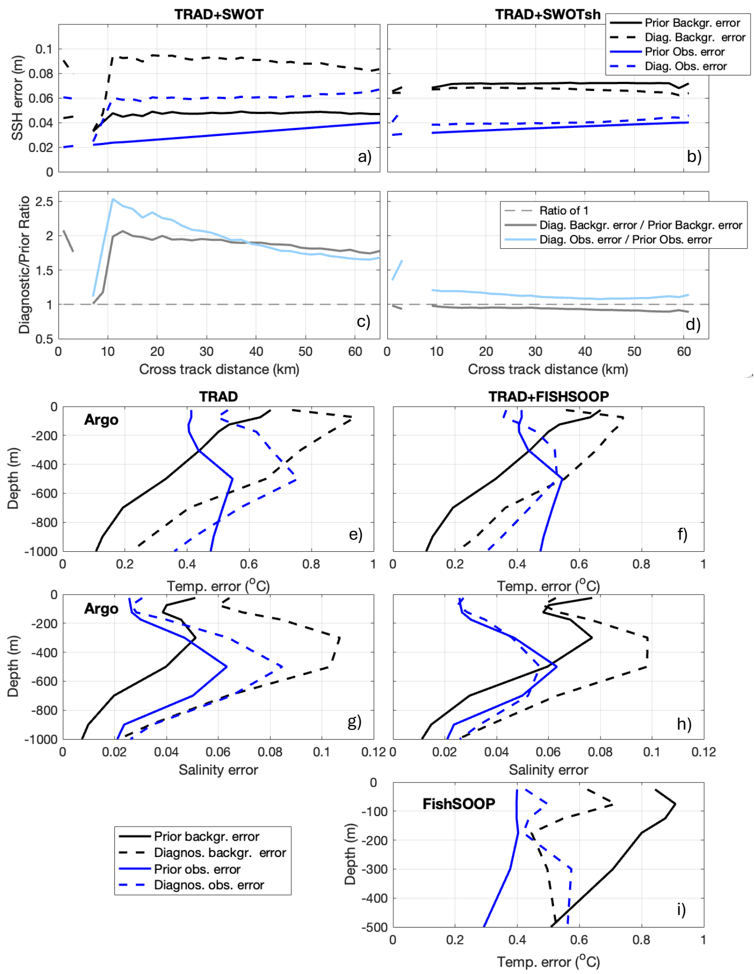

Figure 2. Diagnostic errors and prior observation and background uncertainties for SWOT observations as per Descroziers' equations (Desroziers et al., 2005) as a function of cross-track distance (a,b) and ratios (c,d) for experiments that include SWOT data. Diagnostic errors and prior observation and background uncertainties for in-situ observations as a function of depth for Argo temperature (e,f), Argo salinity (g,h) and FishSOOP observations with QC values 1 and 2 (i).

https://doi.org/10.5194/egusphere-2026-2467
Preprint. Discussion started: 21 July 2026

3 Analysis Performance Results

We begin by assessing the overall performance of the 4D-Var experiments relative to observations. The model analyses are compared to the observations that become available over the assimilation window to quantitatively assess the performance of the model over time. Note that the observations presented in the comparisons are not all assimilated in all experiments (refer to Table 1 and Table 3). Comparing analyses against assimilated observations provides objective assessment of the analysis fit, while comparison to independent observations provides a measure of the system performance away from assimilated data.

A 1-year free-running simulation (Free Run) is presented as a baseline to illustrate the benefit of data assimilation (Table 3). This run is initialized from OceanMAPS on 1 August 2023 and runs freely with no data assimilation over the entire year. The Hot Start experiment is initialised from OceanMAPS every 6-days; data assimilation is performed on the parent model but no data assimilation is performed on the regional ROMS domain. The Hot Start provides a non-assimilating experiment with spin-up of the near-global model on the higher-resolution regional domain over 6-days, and provides a benchmark for the 6 assimilating experiments. For the assimilating experiments, observations are assimilated using 4D-Var over a 6-day time window, with the analysis providing initial conditions for the subsequent 6-day forecast. For the Hot Start and the 6 assimilating experiments, 61 successive 6-day windows make up the 1-year model experiment period.

To assess model skill, we extract the model values at the observation times and locations for all assimilated and independent observations. The domain- and year-averaged model-observation differences (Mean Absolute Difference, MAD) are presented in Table 3. Table 4 summarizes the MAD results from Table 3 in terms of percentage improvement to display the impacts of the updated data assimilation configuration, the updated data assimilation configuration with SWOT data, and the impacts of FishSOOP, SWOT and FishSOOP and SWOT together. The far right column (TRAD+SWOT+FishSOOP compared to TRAD) shows the total improvement achieved through the updated data assimilation configuration, and the inclusion of SWOT and FishSOOP data, in addition to the 'traditionally available' observations.

Spatial plots of model skill at the surface are presented for three chosen experiments (TRADshortTS, TRAD+SWOTsh and TRAD+SWOT+FishSOOP), for all observations over the 1-year period binned into 0.5^o cells (Figure 3a-c). For subsurface observations, observations and the corresponding model values over the 1-year period are binned with depth and we present profiles of the mean, bias, and MAD between the models and the observations, and the number of observations in each depth bin (Figure 3d,e for Argo and Figure 4 for the FishSOOP and all independent subsurface observations). At Argo float times and locations we also compute the mixed layer depth (MLD), and Table 3 displays the Coefficient of Determination (R^2) value associated with the linear fit between modelled and observed MLD, and the MAD. We compute the MLD as the surface duct depth, computed here as the depth at which the sound speed reduces by 0.5 ms^{-1} below the upper-ocean-maximum sound speed.

For SSH observations, the model-observation differences are presented as wave-number spectra to illustrate model fit across scales (Figure 5). Spatial representation of the model-observation differences and the coverage of subsurface temperature observations from Argo and the FishSOOP program are shown in Figure 6, separated into depth ranges representing the upper

https://doi.org/10.5194/egusphere-2026-2467
Preprint. Discussion started: 21 July 2026

ocean including the mixed layer (upper 50 m), the thermocline region (50-400 m) and a region of 100 m above the ocean bottom.

Drogued surface drifters provided current velocity measurements across the model domain over the 1-year period (Figure 1e, Section 2.3.6). As the drifters are drogued at 15 m depth they effectively measure the current velocity integrated over the upper 15 m, so we make comparisons against model velocities integrated over the upper 15 m (upper 3-4 model layers). A simple correction to remove Stokes drift from the drifter velocities is applied, where Stokes drift is estimated as 1% of the wind speed (following Tamtare et al., 2022). Drifter observations representing velocities integrated over the upper 15 m are compared to the modeled velocities at the drifters' corresponding times and locations in Figure 7.

The results are discussed below in the context of the impact of the optimized data assimilation configuration (Section 4), the impact of assimilating SWOT data (Section 5) and the impact of assimilating FishSOOP data (Section 6). Like most studies that assess the performance of a data assimilative system, we present average statistics describing model-observation differences against assimilated and independent observations (in this case over a 1-year period). However, we note that independent observations from gliders and a research cruise observe specific flow structures without widespread spatial and temporal coverage, so spatially and temporally averaged statistics comparing these observations to the different model experiments are not a conclusive way to compare experiments. In Kerry et al. (2026c) we exploit these independent observations to present several specific flow scenarios to elucidate the impact of SWOT and FishSOOP observations in revealing complex fine-scale structures.

https://doi.org/10.5194/egusphere-2026-2467
Preprint. Discussion started: 21 July 2026

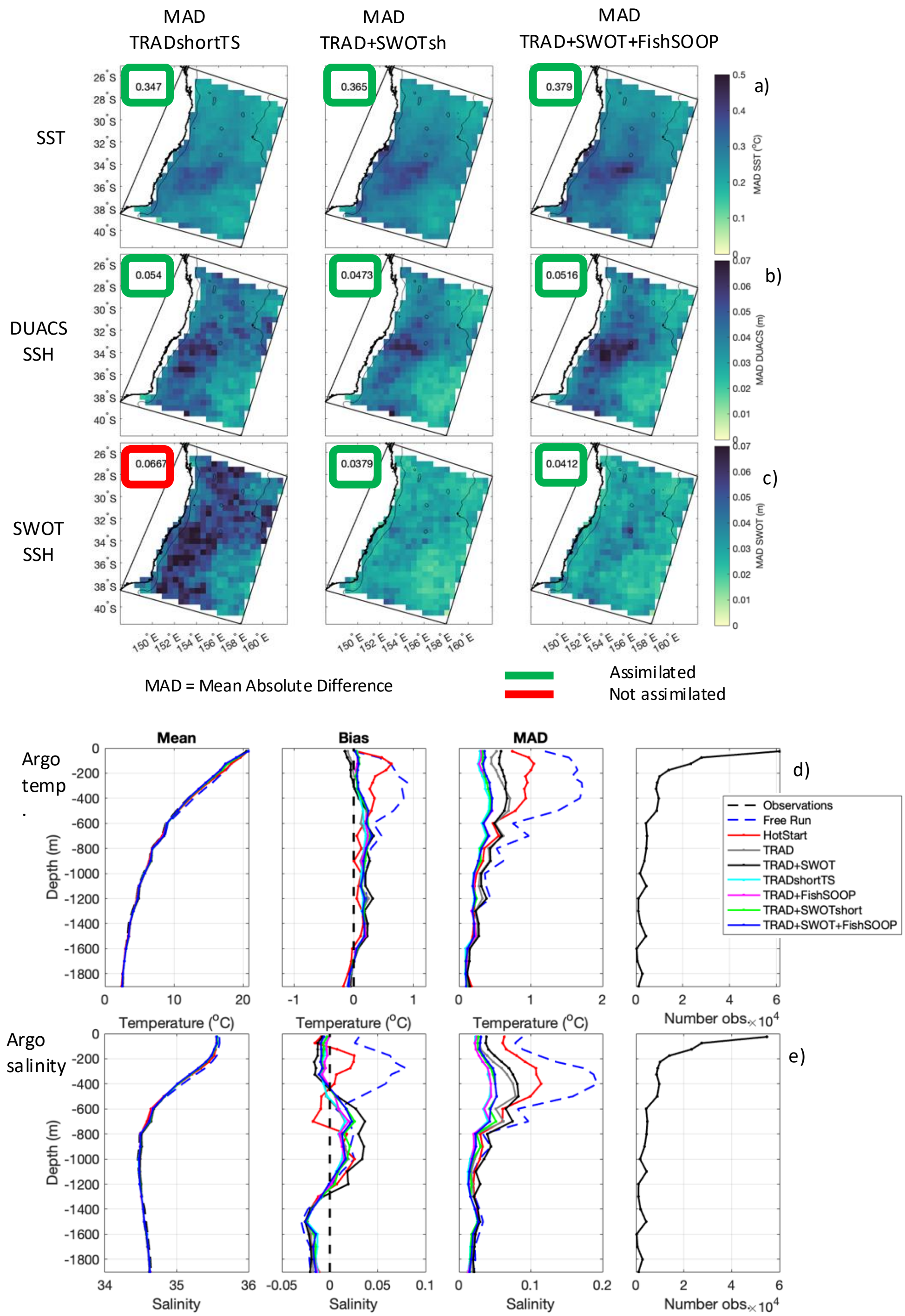

Figure 3. (a-c) Mean Absolute Difference (MAD) for SST (a), DUACS SSH (b) and SWOT SSH (c) for the 3 data-assimilating experiments labelled. Domain-wide MAD is shown in top left corners. (d) Mean temperature observed by Argo floats and mean modelled temperature extracted at all Argo observation locations and times, temperature bias, and MAD between model and observed temperature at all Argo observation locations and times averaged over the assimilation cycles and number of observations per depth bin. (e) Same as (d) but for salinity observed by Argo floats.

https://doi.org/10.5194/egusphere-2026-2467
Preprint. Discussion started: 21 July 2026

Table 3. Fit of all model experiments to assimilated and independent observations. Each cell contains the year-averaged MAD, and whether the observation platform is assimilated (✓) or not (×). For Mixed Layer Depth (MLD) at Argo float times and locations, R^2/MAD are shown.

Model exp.:	Free Run	Hot Start	TRAD	TRAD+ SWOT	TRAD shortTS	TRAD+ FishSOOP	TRAD+ SWOTsh	TRAD+SWOT +FishSOOP
DUACS SSH (cm)	15.8 (×)	9.3 (×)	9.1 (✓)	7.2 (✓)	5.6 (✓)	6.3 (✓)	4.5 (✓)	5.0 (✓)
SWOT SSH (cm)	15.4 (×)	9.6 (×)	10.1 (×)	4.8 (×)	7.0 (×)	7.6 (×)	3.1 (✓)	3.4 (✓)
Midnight SST (^oC)	0.94 (×)	0.53 (×)	0.58 (✓)	0.59 (✓)	0.35 (✓)	0.37 (✓)	0.36 (✓)	0.37 (✓)
Argo temp. (upper 1000 m)	1.20 (×)	0.71 (×)	0.55 (✓)	0.57 (✓)	0.38 (✓)	0.36 (✓)	0.37 (✓)	0.38 (✓)
Argo salinity (upper 1000 m)	0.11 (×)	0.072 (×)	0.050 (✓)	0.060 (✓)	0.032 (✓)	0.033 (✓)	0.039 (✓)	0.039 (✓)
Argo MLD (m)	0.25/28.7 (×)	0.49/25.4 (×)	0.51/19.2 (✓)	0.35/23.0 (✓)	0.59/15.8 (✓)	0.61/16.3 (✓)	0.60/16.5 (✓)	0.62/16.6 (✓)
FishSOOP temp.	1.26(×)	0.93(×)	1.05(×)	1.03(×)	0.92(×)	0.51(✓)	0.88(×)	0.54(✓)
Moana temp. - Cruise	1.38(×)	1.10(×)	0.89(×)	0.94(×)	0.73(×)	0.80(×)	0.79(×)	0.87(×)
Glider temp.	1.37(×)	1.19(×)	1.67(×)	1.58(×)	1.40(×)	1.41(×)	1.67(×)	1.27(×)

https://doi.org/10.5194/egusphere-2026-2467
Preprint. Discussion started: 21 July 2026

Table 4. Percentage improvement (%) based on the MADs from Table 3. The MAD is the domain- and year-averaged MAD between the observations (platforms in left colum) and the model experiment (sampled at observation times and locations). The percentage improvement in MAD between Exp_2 vs Exp_1 is $((MAD_1 - MAD_2)/MAD_1) \times 100$. A positive number refers to improvement in the fit to that observation platform, while a negative number refers to a degradation in the fit. The model experiments compared are given in the top row, with explanation of what the comparison shows. For example, comparing TRADshortTS and TRAD shows the impact of the updated DA configuration (given assimilation of 'traditionally available' observations). Comparing TRAD+SWOTsh and TRADshortTS shows the impact of SWOT data (given the updated DA configuration). The last column shows the total improvement achieved through the updated DA configuration and the inclusion of SWOT and FishSOOP data (in addition to the 'traditionally available' observations). DA = data assimilation. We show whether the observation platform is assimilated in both experiments ($\checkmark$), in neither experiment ($\times$), or in the first experiment but not the second ($\sim$).

Impact:	Updated DA config (TRADshortTS vs TRAD)	Updated DA config. with SWOT (TRAD+SWOTsh vs TRAD+SWOT)	FishSOOP impact (TRAD+FishSOOP vs TRADshortTS)	SWOT impact (TRAD+SWOTsh vs TRADshortTS)	FishSOOP and SWOT impact (TRAD+SWOT+ FishSOOP vs TRADshortTS)	Total improvement (TRAD+SWOT+ FishSOOP vs TRAD)
DUACS SSH (cm)	38.5 ($\checkmark$)	37.5 ($\checkmark$)	-12.5 ($\checkmark$)	19.6 ($\checkmark$)	10.7 ($\checkmark$)	45.1 ($\checkmark$)
SWOT SSH (cm)	30.7 ($\times$)	35.5 ($\checkmark$)	-8.6 ($\times$)	55.7 ($\sim$)	51.4 ($\sim$)	66.3 ($\sim$)
Midnight SST (^oC)	39.7 ($\checkmark$)	39.0 ($\checkmark$)	-5.7 ($\checkmark$)	-2.9 ($\checkmark$)	-5.7 ($\checkmark$)	36.2 ($\checkmark$)
Argo temp. (upper 1000 m)	30.9 ($\checkmark$)	35.5 ($\checkmark$)	5.3 ($\checkmark$)	2.6 ($\checkmark$)	0.0 ($\checkmark$)	30.9 ($\checkmark$)
Argo salinity (upper 1000 m)	36.0 ($\checkmark$)	35.0 ($\checkmark$)	-3.1 ($\checkmark$)	-21.9 ($\checkmark$)	-21.9 ($\checkmark$)	22.0 ($\checkmark$)
Argo MLD (m)	17.7	28.3	-3.2	-4.4	-5.1	13.5
FishSOOP temp.	12.4 ($\times$)	14.6 ($\times$)	44.6 ($\sim$)	4.3 ($\times$)	41.3 ($\sim$)	48.6 ($\sim$)
Moana temp. - Cruise	18.0 ($\times$)	16.0 ($\times$)	-9.6 ($\times$)	-8.2 ($\times$)	-19.2 ($\times$)	2.3 ($\times$)
Glider temp.	16.2 ($\times$)	-5.7 ($\times$)	-0.7 ($\times$)	-19.3 ($\times$)	9.3 ($\times$)	24.0 ($\times$)

https://doi.org/10.5194/egusphere-2026-2467
Preprint. Discussion started: 21 July 2026

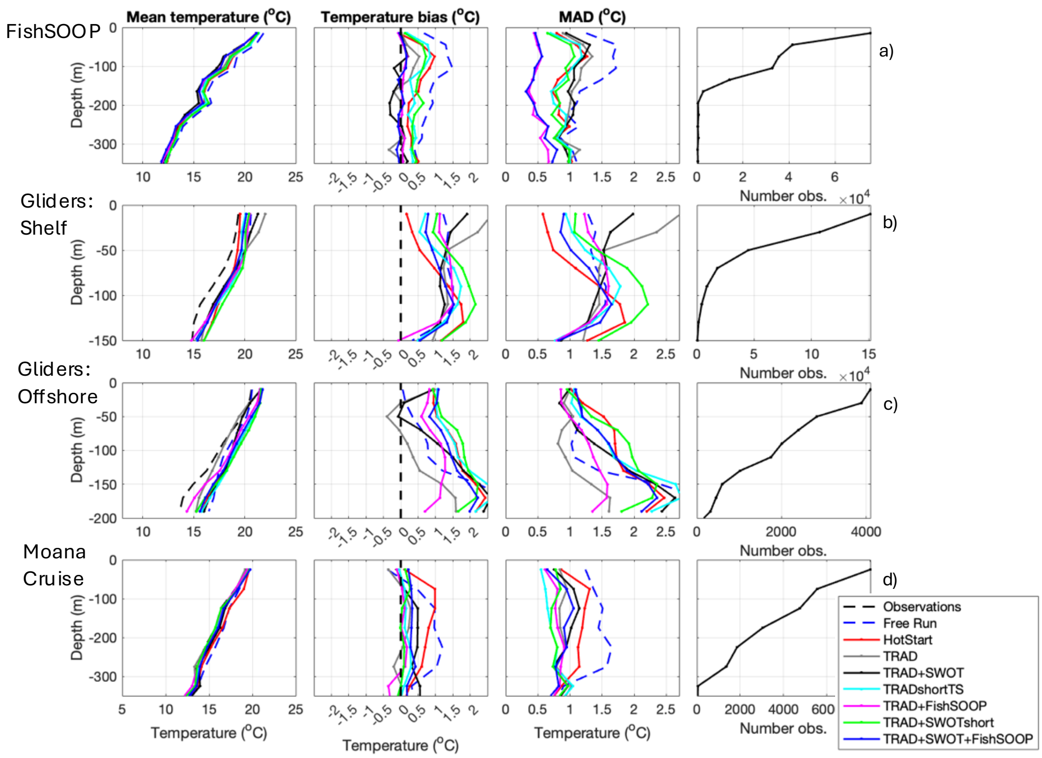

Figure 4. a) Mean FishSOOP temperature observations and mean modelled temperature extracted at all FishSOOP observation locations and times, temperature bias, MAD between model and observed temperature at all FishSOOP observation locations and times averaged over the assimilation cycles, and number of observations per depth bin. (b) Same as (a) for Glider observations on the continental shelf (water depths <1000 m). (c) Same as (a) for Glider observations offshore of the continental shelf (water depths >1000 m). (d) Same as (a) for Moana Cruise observations. Note that the vertical axis limits vary between rows.

https://doi.org/10.5194/egusphere-2026-2467
Preprint. Discussion started: 21 July 2026

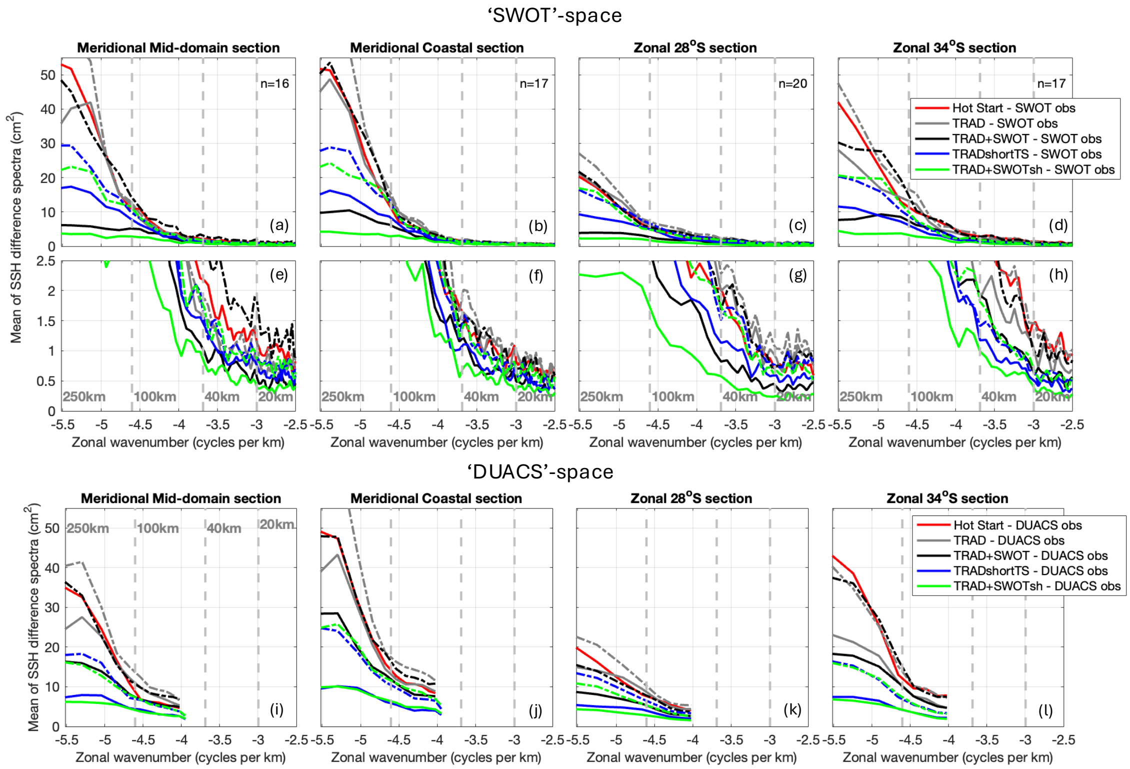

Figure 5. (a-d) Skill in 'SWOT-space'. Mean of the *n* wavenumber spectra on absolute difference between SWOT SSH observations and modeled values for meridional mid-domain section, meridional coastal section, and two zonal sections (sections shown in Figure 1c). For the assimilating experiments, solid lines refer to the analyses and dot-dashed lines refer to the forecasts. (e-h) are equivalent to (a-d) but with different y-axis limits to reveal error differences at the fine-scales.(i-l) Skill in 'DUACS-space'. Mean of the daily wavenumber spectra on absolute difference between DUACS SSH observations and modeled values for the same four sections. The mean SSH error spectra are presented in a variance-preserving form (Emery and Thompson, 2001). Ensemble and band averaging (2 ensembles and 2 bands) are applied to increase the statistical significance of each spectra. The x-axis limits are 250 km - 12 km; DUACS data only resolves wavelengths > 54 km. Note the x-axes are log scale; log(1/250 km)=-5.5, log(1/12 km)=-2.5.

https://doi.org/10.5194/egusphere-2026-2467
Preprint. Discussion started: 21 July 2026

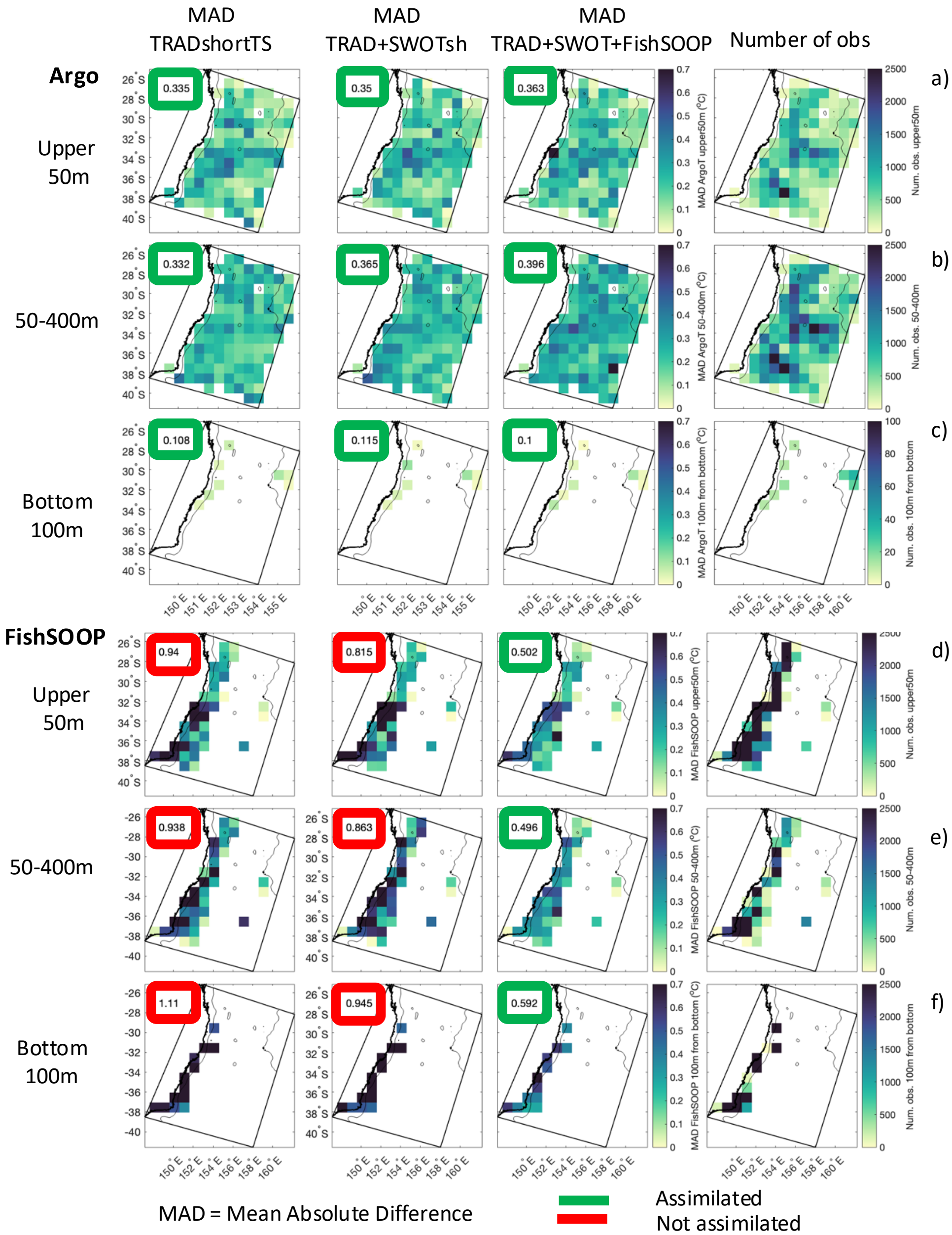

Figure 6. Mean Absolute Difference (MAD) and observation coverage for Argo (a-c) and FishSOOP (d-f). MAD and number of observations are shown for depth ranges 0-50 m, 50-400 m, and 100 m above the bottom. Domain-wide MAD is shown in top left corners.

https://doi.org/10.5194/egusphere-2026-2467
Preprint. Discussion started: 21 July 2026

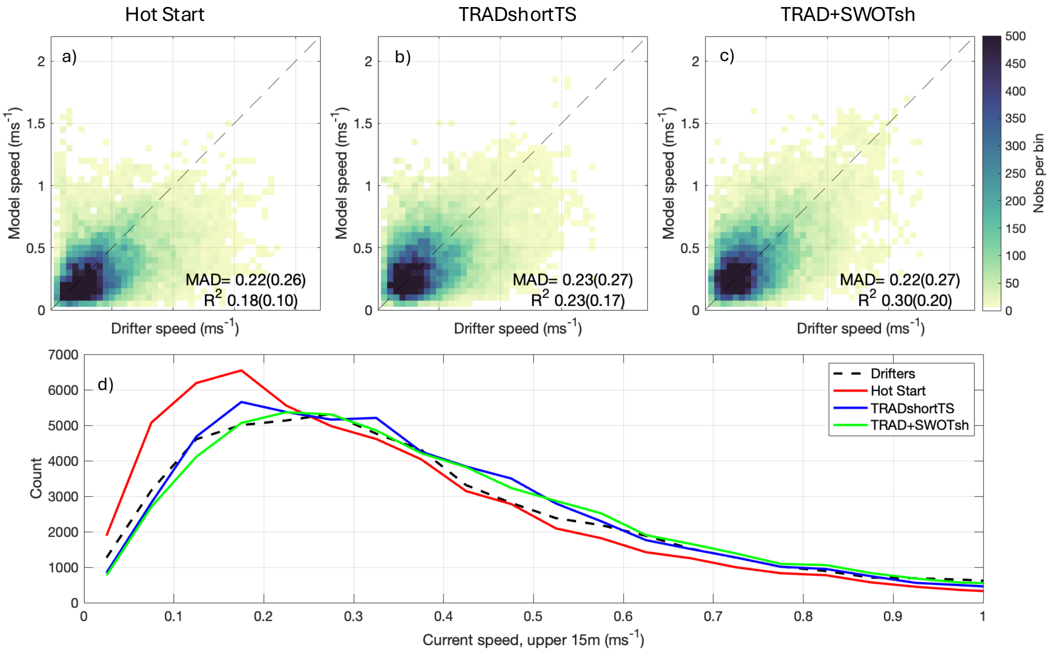

Figure 7. Comparison of drifter speed and model speed, depth integrated over the upper 15 m and extracted at the drifter times and locations, for Hot Start (a), TRADshortTS (b) and TRAD+SWOTshort (c). Coefficient of Determination (R^2) values for all observations (and for only speeds >0.5 ms^{-1}) are shown. (d) Distribution of drifter speeds and model speeds.

4 Impact of Optimized Data Assimilation Configuration

All of the data assimilating experiments and the Hot Start (where forecasts are intialized every 6-days from a data-assimilating parent domain) provide improvement compared to the Free Run across all assimilated and independent observations (Table 3). The exception is the (isolated) glider observations (discussed below). The TRAD experiment showed marginal to no improvement compared to the Hot Start at the surface; however, assimilation of ‘traditionally available’ observations on the higher resolution domain provided improvements in representation at Argo float locations (Table 3). Compared to the Free Run (Hot Start), TRAD showed improvements of 54% (23%) for Argo temperature, 55% (31%) for Argo salinity, and 33% (24%) for the mixed layer depth at Argo float locations. TRAD+SWOT provided improvement in SSH representation compared to the Hot Start (23% for DUACS and 50% for SWOT), with similar model-observation differences to TRAD for SST and Argo observations.

Further improvement was achieved with updated prior observation and model background uncertainty estimates (in TRADshortTS, TRAD+FishSOOP, TRAD+SWOTsh and TRAD+SWOT+FishSOOP). These changes to the data assimilation configuration (presented in Section 2.6, Table 1, Table 2, Figure 2) translate to considerable improvement in the model fit to both assimilated surface and subsurface observations and to independent in situ observations (Table 3, Table 4). Assimilating the same observations as TRAD, TRADshortTS shows improvements (compared to TRAD) for DUACS SSH, SWOT SSH, SST,

https://doi.org/10.5194/egusphere-2026-2467
Preprint. Discussion started: 21 July 2026

Argo temperature, Argo salinity and Argo MLD of 39%, 31%, 40%, 31%, 36% and 18% respectively. In situ subsurface temperature observations from FishSOOP, the Moana sensors used on the research cruise and the Gliders are all independent to both TRAD and TRADshortTS, and the latter gives improvements of 12%, 18% and 16% respectively.

The depth structure of the model-observation differences for Argo observations (Figure 3d-e) show improvement in the upper ocean from the Free Run and Hot Start with TRAD and TRAD+SWOT, and further improvement for the optimized configurations (TRADshortTS, TRAD+FishSOOP, TRAD+SWOTshort and TRAD+SWOT+FishSOOP). The FishSOOPobservations cover the coastal and near-shelf region and are wide-spread in space and time over the 1-year simulation (Figure 1d,g), providing independent observations for TRAD, TRAD+SWOT, TRADshortTS and TRAD+SWOTsh. Compared against FishSOOP observations, the optimized configuration of TRADshortTS gives improvement of 12% (compared to TRAD), and TRAD+SWOTsh gives 15% improvement compared to TRAD+SWOT (Table 3, Table 4, Figure 4a).

Most glider observations are confined to a region over the continental shelf (water depths <1000 m) between 32-34^{o}S, although one mission extended off the shelf from 34-38^{o}S from 31-Oct-2023 to 17-Nov-2023 (Figure 1e,g). We separate the model-glider comparisons into on- and off-shelf (Figure 4b-c). TRAD and TRAD+SWOT exhibit a warm bias and higher model-observation differences for shelf observations, compared to all other experiments. These results suggest that shorter decorrelation length scales associated with the background uncertainty covariance matrix are beneficial in representing independent shelf observations, consistent with results of Kerry et al. (2024a). Because the off-shelf glider observations represent a single track (that runs approximately north-south from 34-38^{o}S from 31-Oct-2023 to 17-Nov-2023) it is difficult to ascertain overall model performance due to complexities of subsurface structure; detailed comparison is presented in Kerry et al. (2026c). In situ temperature observations taken by Moana sensors aboard the RV investigator research cruise measured several fronts and cross sections through eddies over 3 weeks in Oct-2023 (Figure 1e,g). These observations specifically targeted fronts and eddies: TRADshortTS shows an improvement of 18% compared to TRAD, and TRAD+SWOTsh an improvement of 16% compared to TRAD+SWOT (Table 3, Table 4, Figure 4d).

Using SWOT and DUACS observations, we are able to show the improved model representation of SSH across scales (Figure 5), particularly for TRADshortTS compared to TRAD, and TRAD+SWOTsh compared to TRAD+SWOT. Comparison of TRAD and TRAD+SWOT (as presented in Kerry et al., 2026a) show that while TRAD+SWOT provides considerably improved analysis skill when compared to SWOT data, forecast skill for TRAD+SWOT is comparable to the TRAD experiment for scales <100 km for the meridional coastal and two zonal sections, and exhibits higher forecast errors compared to TRAD for the meridional mid-domain section at scales <100 km. This reveals that assimilating SWOT provides little additional skill (compared to TRAD) in predicting where the fine-scale features will occur during the subsequent SWOT passes. The results with the optimized data assimilation configuration (comparing TRADshortTS and TRAD+SWOTsh) are consistent with this, albeit with considerably better analysis and forecast skill across scales (Figure 5a-h). In 'SWOT-space', TRAD+SWOTsh provides improved analysis and forecast skill compared to TRADshortTS for the large scales (>100 km) but similar forecast skill for the fine-scales (<100 km).

The DUACS observations provide mesoscale-resolving (>54 km) gridded daily fields through mapping of the altimeter data, and the effective temporal resolution is 10-30 days (Pujol et al., 2016). As such, error analysis in 'DUACS-space' refers to

https://doi.org/10.5194/egusphere-2026-2467
Preprint. Discussion started: 21 July 2026

representation of the large-scale slowly-evolving mesoscale SSH field. Prior to system optimization, TRAD+SWOT provided improved analysis and forecast skill against DUACS observations compared to TRAD, except across the eddy-dominated 34^{o}S section where forecast skill was similar. With updated specification of the prior observation and background uncertainties, the model that assimilates SWOT (TRAD+SWOTsh) provides a more subtle improvement in analysis and forecast skill for the resolved scales (>54 km), compared to the one that does not include SWOT (TRADshortTS, Figure 5i-l). This highlights the importance of an optimised system in improving forecast skill, with system optimization (TRADshortTS compared to TRAD) giving greater improvement in forecast skill than inclusion of SWOT data in the sub-optimal system (TRAD+SWOT compared to TRAD).

5 Impact of assimilating SWOT sea surface height observations

Assimilation of SWOT data considerably improves the fit to SWOT observations (as expected) and also improves the fit to the DUACS SSH data by 21% (for TRAD+SWOT compared to TRAD) and by 20% (for TRAD+SWOTsh compared to TRADshortTS, Table 3, Table 4). Figure 3 reveals higher errors (MAD) in the eddy-domianted region for SST and DUACS SSH. Reduction in DUACS SSH errors with assimilation of SWOT is predominantly around the EAC separation region (Figure 3b, TRAD+SWOTsh compared to TRADshortTS). Consistent with Kerry et al. (2026a), assimilation of SWOT data (in TRAD+SWOTsh) improves analysis skill across-scales (compared to TRADshortTS, Figure 5) and improves forecast skill for scales >100 km. Even with the updated system configuration (TRAD+SWOTsh and TRADshortTS, compared to suboptimal TRAD+SWOT and TRAD), the forecast skill of the fine-scale rapidly-evolving SSH features resolved by SWOT is not improved with the assimilation of SWOT. That is, forecast skill in 'SWOT-space' remains comparable in TRAD+SWOTsh and TRADshortTS (Figure 5e-h, blue and green dashed lines). In contrast, for the slowly-evolving mesoscale field, system optimization provides considerable benefits to analysis and forecast skill (Figure 5i-l). The benefit of system optimization in terms of forecast skill for the mesoscale (in 'DUACS-space') outweighs the benefit of assimilating SWOT observations (TRADshortTS provides better forecasts of the large-scale SSH field than TRAD+SWOT).

Assimilating SWOT data introduces additional fine-scale variability that better matches observed variability, and improves the subsurface representation of fronts, introducing sharper relativity vorticity gradients that better represent observed gradients (as shown by Kerry et al., 2026a). Here we assess the impact of assimilating SWOT on subsurface temperature representation using FishSOOP observations that provide high resolution data in the coastal and shelf regions. The FishSOOP observations are independent to TRADshortTS and TRAD+SWOTsh and, over the 1-year period, provide widespread coverage in space and time (Figure 1d,g, Figure 6d-f) making them representative independent observations for objective model assessment. The improvement in subsurface temperature representation as measured by FishSOOP observations for TRAD+SWOTsh compared to TRADshortTS is 13%, 8%, and 15% for observations in the upper 50 m, 50-400 m depth range, and observations 100 m above the bottom, respectively (Figure 6d-f). The upper 50 m and 50-400 m depth ranges are chosen to represent the mixed layer and thermocline regions, respectively. The depth range of 100 m above the bottom was chosen to highlight the improvements to near bottom temperature, noting that some overlap may exist between the depth ranges for water depths <500 m.

https://doi.org/10.5194/egusphere-2026-2467
Preprint. Discussion started: 21 July 2026

The distribution of current speeds across all drifter observations and the corresponding model values (Figure 7d) shows that the TRAD+SWOTsh model provides the best match to the observed distribution. TRADshortTS also provides a close match, while the Hot Start model distribution is skewed towards lower current speeds. Higher current speeds are associated with sharper sea surface height gradients when assimilation is performed on the high-resolution grid (TRADshortTS) and further with the inclusion of SWOT data (TRAD+SWOTsh). Plots of model speed against drifter speed (Figure 7a-c) show an improved fit for the model that assimilates SWOT. The Mean Absolute Differences for model and observed velocities are similar for the three model experiments presented, but the Coefficient of Determination (R^2) is greater from Hot Start to TRADshortTS to TRAD+SWOTsh. The R^2 value represents the proportion of variance in the observed velocities that is explained by the modelled velocities. The TRADshortTS model predicts an additional 5% of the total variance compared to the Hot Start model (computed across all current speeds), and the TRAD+SWOTsh model predicts an additional 12% (compared to Hot Start) and an additional 7% compared to TRADshortTS.

6 Impact of assimilating FVON / FishSOOP subsurface temperature observations

FishSOOP provides a step-change in subsurface temperature data availability in the coastal and shelf region off southeastern Australia (Figure 6d-f) compared to Argo (Figure 6a-c). The FishSOOP observations are assimilated in two different experiments, firstly in concert with the traditional observations (DUACS SSH, SST and Argo - TRAD+FishSOOP) and secondly with the traditional observations and SWOT SSH (TRAD+SWOT+FishSOOP). Both TRAD+FishSOOP and TRAD+SWOT+FishSOOP use the optimized data assimilation configuration as discussed in Section 2.6. When compared with FishSOOP observations, TRAD+FishSOOP and TRAD+SWOT+FishSOOP exhibit very little bias and considerable reduction in MAD compared to the other experiments (Figure 4a). The overall improvement in MAD for TRAD+FishSOOP compared to TRADshortTS is 45% and for TRAD+SWOT+FishSOOP compared to TRAD+SWOTsh is 39% (Table 3, Table 4). Across three chosen depth ranges, Figure 6d-f shows that assimilation of FishSOOP data provides considerably improved representation of subsurface temperature in coastal and shelf regions (TRAD+SWOT+FishSOOP compared to TRADshortTS and TRAD+SWOTsh). The overall improvement in subsurface temperature representation as measured by FishSOOP observations for TRAD+SWOT+FishSOOP compared to TRADshortTS (and TRAD+SWOTsh) is 47% (38%) for the upper 50 m depth range, 47% (43%) for the 50-400 m depth range and 47% (37%) for the observations 100 m above the bottom.

There is some degradation in the fit to surface observations with the inclusion of FishSOOP data (Table 3, Table 4), which is common when the system must fit to more data streams (e.g. Siripatana et al., 2020). However, the spatial structure of the surface errors (Figure 3) is similar for TRAD+SWOTsh and TRAD+SWOT+FishSOOP. Over-fitting to FishSOOP observations could result in changes to the spatial structure of errors (e.g. Kerry et al., 2024a), which is not the case here. Ratios of diagnostic errors and prior observation and background uncertainties for TRAD+FishSOOP and TRAD+SWOT+FishSOOP are very close to unity (for FishSOOP observations with QC values of 1 and 2, Table 2) indicating a near optimal fit. For FishSOOP observations with high location uncertainty (QC values of 3) the ratios indicate underfitting; however the inflated observation uncertainty estimates are justified by the high location uncertainty and the sharp spatial gradients that exist in the region.

https://doi.org/10.5194/egusphere-2026-2467
Preprint. Discussion started: 21 July 2026

While the FishSOOP data over the 1-year period provide good coverage of the coastal and shelf region off southeastern Australia, the independent observations (glider and Moana sensor data) are more isolated in time and space and therefore less representative of overall performance. As such, comparisons of the model experiments with glider and Moana sensor observations from the cruise do not provide conclusive results regarding the impact of FishSOOP data (Figure 4b-d). In Kerry et al. (2026c) we explore specific case studies to elucidate differences across the model experiments. We show that assimilation of FishSOOP observations provides sustained positive impact on subsurface temperature representation over time, even at times when FishSOOP data is not available.

Because the temperature sensors are attached to fishing equipment, the structure of the data (i.e. how the sensor moves through the water column in time and space) depends on the specific equipment (e.g. Jakoboski et al., 2024, their Fig. 5). By using the time-dependent 4D-Var data assimilation scheme, observations can be assimilated at the times and locations that they are taken, with the data assimilation scheme taking into account the time-dependent flow over the assimilation window. This allows the observations to provide added value, compared to a time-independent scheme (such as 3DVar, ENOI) in which more spatial and temporal averaging of the observations would be required before combining them with the model. For example, when fishing equipment crosses sharp fronts (which they often do when fishers target temperature fronts as foraging regions in the ocean) the high spatial and temporal variability can be ingested into the data assimilating model. In Kerry et al. (2026c) we present a scenario where FishSOOP data observes a sharp temperature front and improves model representation of the complex subsurface structure.

As FishSOOP data location information comes from the vessel rather than the temperature sensor itself, for fishing activity such as long-line fishing where the equipment can be a considerable distance from the vessel, uncertainty on the location of the temperature sensors can be high (>50 km). The exception is when the equipment is known to be close to the vessel on deployment (the descending profile) and recovery (the ascending profile). As mentioned in Section 2.6.1, for FishSOOP observations with high location uncertainty (QC=3), prior observation uncertainty estimates were inflated such that the observations are not fit as tightly. Future FishSOOP data products should aim to separate the descending and ascending profiles where positional accuracy is high, and subsequently apply different quality control flags, to allow more value to be drawn from the observations taken close to the long-line vessels.

7 Conclusions

The combination of observations of coastal, shelf and marginal seas with regional ocean models to produce data-constrained, four-dimensional oceanographic fields supports a wide range of socioeconomic needs (e.g. Edwards et al., 2024). The observations are necessarily sparse in space and/or time due to practical limitations, relative to the scales of variability of the ocean dynamics one is aiming to resolve. Data from new observation platforms, such as SWOT and FVON / FishSOOP studied here, present new opportunities in terms of resolving and representing (in model state estimates) finer-scale features and complex subsurface structure. Appropriate hydrodynamic models and data assimilation systems are required in order to exploit such observations.

https://doi.org/10.5194/egusphere-2026-2467
Preprint. Discussion started: 21 July 2026

Here we used a submesoscale-permitting regional model of a highly dynamic WBC region and 4D-Var data assimilation to assess the value of SWOT and FVON / FishSOOP observations on model state estimates. Using a well-tested modelling and data assimilation configuration of the EAC system, we present an optimization strategy for the data assimilation configuration and demonstrate the positive impact of both SWOT and FishSOOP observations on surface and subsurface ocean state estimates. The updated configuration gives improvements in the fit of the analyses to the observations of 30-40% for assimilated observations and 12-15% for independent FishSOOP observations (Table 4). Assimilation of high density FishSOOP data significantly improves subsurface temperature representation in coastal and shelf regions (by 41-45%, Table 4). The assimilation of SWOT data improves the fit by 20% for DUACS SSH and 56% for SWOT SSH. The total improvement achieved through the updated data assimilation configuration and the inclusion of SWOT and FishSOOP data (in addition to the 'traditionally available' observations) is 36-66% for surface observations, 31% and 22% for Argo temperature and salinity in the upper 1000 m, and 49% for FishSOOP observations (Table 4, right column).

We show that inclusion of SWOT data improves model representation of sea surface height across scales, and also improves representation of independently observed subsurface temperature in the coastal and shelf regions, and surface velocities. Assimilating SWOT data in our model configurations improves representation of sea surface height at mesoscales and finer spatial scales (in the analyses), and system optimization provides considerable improvements to analysis skill as compared to SWOT observations across scales. However, the forecast skill of the fine-scale rapidly-evolving SSH features resolved by SWOT is not improved with the assimilation of SWOT; this is the case for the original configurations (as in Kerry et al., 2026a) and the updated (improved) system configurations. In contrast, for the slowly-evolving mesoscale field, system optimization provides considerable benefits to both analysis and forecast skill. In terms of forecast skill for the large-scale SSH field, the benefit of system optimization outweighs the benefit of assimilating SWOT observations.

SWOT observations were shown to impact state estimates below the surface. In Kerry et al. (2026a) the impact of assimilating SWOT data was shown to be projected to depth, introducing sharper vorticity gradients that better matched (independently) observed gradients. Here we show that SWOT observations improve the fit to high-resolution subsurface temperature observations as observed by (independent) FVON / FishSOOP observations across all depth ranges (by 8-15%). Assimilation of FVON / FishSOOP data provides significant further improvement (37-47% total improvement), highlighting the value of collecting these subsurface observations in collaboration with the fishing community in previously under-observed coastal and shelf regions. Future work aims to assimilate the data collected by fishing vessels into real-time forecasts (SEA-COFS) that can be used by the fishermen; such a win-win relationship was demonstrated by Hirose et al. (2024) in Japan.

Our results show that the impact of observations is dependent on the data assimilation system configuration. Indeed, the effective combination of observations and models requires an effective data assimilation system that allows the new model estimate (the analysis) to represent the observations by placing them in dynamical context. The difference in data assimilation techniques lies in the way by which the information contained in the observations is projected into model space to produce the new state estimate. This is controlled by the background error covariance matrix which carries the statistical information of the model prior and determines the spatial and temporal structure of the adjustments. Further, for a given data assimilation

https://doi.org/10.5194/egusphere-2026-2467
Preprint. Discussion started: 21 July 2026

methodology, the optimality of model estimates and forecasts is strongly dependent on prior assumptions of the background and observation uncertainties (Moore et al., 2019).

In classic 4D-Var used here, the model background covariances are assumed to be static with isotropic horizontal and vertical length scales and the tangent-linear and adjoint models introduce flow-dependence via the time evolution of the background. The standard deviations provide a measure of the expected uncertainty in the model background, and the horizontal and vertical decorrelation length scales provide an estimate of the spatial extent that information from the observations should impact the model state. As such, configuring a classic 4D-Var system requires assumptions around observation uncertainties, and the standard deviations and length scales used to compute the background error covariance matrix. Here we have shown that adjustments to the prior assumptions of observation and background uncertainties, and the assumed decorrelation length scales, can significantly impact (improve) model skill as compared to both assimilated and independent observations.

The considerable improvement in model skill highlights the importance of system optimization, and also motivates future work into further improving data assimilation schemes. Specifically, it is likely that for highly variable flows with sharp spatial gradients, flow-dependent covariances are beneficial over horizontally isotropic and temporally invariant covariances as they can describe error correlation patterns that stretch out along fronts for example. Flow-dependent covariances can be achieved through the merging of 4D-Var and ensemble methods; this hybrid approach has been noted as the most immediate development being borrowed from Numerical Weather Prediction for ocean data assimilation (Moore et al., 2019). Such ensemble-variational methods have shown improvements in forecast skill in atmospheric applications, particularly in dynamically active systems (e.g. Raynaud et al., 2011; Lorenc and Jardak, 2018).

In terms of observation uncertainty estimates, further work is required to address optimal error specification for SWOT data assimilation, including the consideration of correlated errors (Gille et al., 2025) and quantification of processes that may be captured by the observations but unresolved in the model (e.g. Tréboutte et al., 2023; Dibarboure et al., 2025). A challenge with FVON / FishSOOP observation error estimates relates to uncertainty of the location of the sensor, which can be high if fishing equipment is deployed away from the vessel. Location uncertainty can result in high observation uncertainty, particularly in highly variable regions with sharp oceanic fronts. This will need to be addressed by the FVON community in order to improve the value of the fishing vessel based observations in regions where longlining activity is high and observations are sparse (e.g. the Central Western Pacific).

Overall, we have presented a data assimilation system that is carefully configured and draws value from novel SWOT and FVON / FishSOOP observations to improve model state estimates of the EAC System across spatial scales and below the surface. The results motivate the sustained collection of novel observations and their integration into regional ocean models to provide advances in prediction. Our work also demonstrates the benefit of tight collaboration between observational data collection (e.g FishSOOP) and ocean data assimilation (e.g. SEA-COFS) for continued improvement of both fields of research.

Data availability.

https://doi.org/10.5194/egusphere-2026-2467
Preprint. Discussion started: 21 July 2026

The experimental settings used for this study, including model forcing and configuration files, and a frozen version of the ROMS code used, are published to Kerry et al. (2026b), https://doi.org/10.5281/zenodo.20077064.

The SWOT data is provided by AVISO/DUACS (2024). DUACS SSH data is provided by E.U. Copernicus Marine Service CMS (2024). SST, Argo, FishSOOP and glider data sourced from from Australia's Integrated Marine Observing System (https://imos.org.au/data). Data from the CSIRO Marine National Facility Voyage IN2023_V06 is sourced from here: https://www.marine.csiro.au/data/trawler/survey_details.cfm?survey=IN2023_V06. Drifter data was sourced from here: https://osmc.noaa.gov/erddap/tabledap/OSMC_flattened.html

The Regional Ocean Modelling System (ROMS) is an open-source modelling framework available for download at https://www.myroms.org. This study uses version 4.2.

Author contributions. CK developed the ROMS model configuration of the EAC system, processed the observations, developed and optimised the 4D-Var data assimilation configuration. CK analysed the results, generated the figures and wrote the manuscript. MR and SK secured the funding. MR played a key role in developing the FishSOOP program. SK provided guidance on SWOT. GB provided guidance on data assimilation methodologies. All authors reviewed the analysis methods and contributed to the structure of the manuscript.

Competing interests. No competing interests are present.

Acknowledgements. This research was supported by Australian Research Council grants LP220100515 and DP2301000505. Prior model development was supported by Australian Research Council grants DP140102337, LP160100162 and LP170100498. The research cruise on the RV Investigator was supported by a grant of sea time (IN2023_V06) from the CSIRO Marine National Facility (https://ror.org/01mae9353, https://doi.org/10.13039/501100014536). We thank the crew, officers, support staff and volunteer scientists for their dedication and support. Synchronous SWOT-cruise planning support was provided by the NASA-CNES SWOT Science Team and the SWOT Adapt-a-Crossover Consortium. Australia's Integrated Marine Observing System (IMOS) is enabled by the National Collaborative Research Infrastructure Strategy (NCRIS). It is operated by a consortium of institutions as an unincorporated joint venture, with the University of Tasmania as Lead Agent. We thank the Australian Bureau of Meteorology for providing OceanMAPS ocean forecasts, ACCESS atmospheric forecast products and drifters deployed during the cruise. Compute resources from UNSW's National Compute Infrastructure Resource Allocation Scheme were used: doi 10.26190/PMN5-7J50. We thank V. Lago for providing guidance on the FishSOOP data processing and quality control and L. Matisons for providing guidance on the drifter data processing and quality control.

https://doi.org/10.5194/egusphere-2026-2467
Preprint. Discussion started: 21 July 2026

References

Archer, M. R., Li, Z., Wang, J., and Fu, L.-L.: Reconstructing fine-scale ocean variability via data assimilation of the SWOT pre-launch in situ observing system, Journal of Geophysical Research: Oceans, 127, e2021JC017 362, 2022.

AVISO/DUACS: SWOT level-3 KaRIn low rate SSH expert (v1.0), https://doi.org/10.24400/527896/A01-2023.018, 2024.

Azaneu, M. V., Roughan, M., Keating, S. R., Schaeffer, A., and Schallenberg, C.: Characterising submesoscale processes, uplift and subduction across diverse fronts in the East Australian Current System, Progress in Oceanography, p. 103690, 2026.

Azevedo Correia de Souza, J. M. and de Godoi Rezende Costa, C.: An Assessment of the Moana Operational Forecast System Assimilating Innovative Mangōpare Fishing Vessel Observations in Aotearoa, New Zealand, Journal of Marine Science and Engineering, 14, 591, 2026.

Bonaduce, A., Benkiran, M., Remy, E., Le Traon, P. Y., and Garric, G.: Contribution of future wide-swath altimetry missions to ocean analysis and forecasting, Ocean Science, 14, 1405–1421, 2018.

Brassington, G. B., Sakov, P., Divakaran, P., Aijaz, S., Sweeney-Van Kinderen, J., Huang, X., and Allen, S.: OceanMAPS v4.0i: a global eddy resolving EnKF ocean forecasting system, in: OCEANS 2023-Limerick, pp. 1–8, IEEE, 2023.

Broquet, G., Edwards, C. A., Moore, A., Powell, B. S., Veneziani, M., and Doyle, J. D.: Application of 4D-Variational data assimilation to the California Current System, Dynam. Atmos. Oceans, 48, 69–92, 2009.

Cetina Heredia, P., Roughan, M., Van Sebille, E., and Coleman, M.: Long-term trends in the East Australian Current separation latitude and eddy driven transport, J. Geophys. Res., 119, https://doi.org/10.1002/2014JC010071, 2014.

Chelton, D. B.: A postlaunch update on the effects of instrumental measurement errors on SWOT estimates of sea surface height, velocity, and vorticity, Journal of Atmospheric and Oceanic Technology, 41, 865–888, 2024.

CMS: Global Ocean Gridded L 4 Sea Surface Heights And Derived Variables Reprocessed 1993 Ongoing, https://doi.org/https://doi.org/10.48670/moi-00148, 2024.

D'Addezio, J. M., Smith, S., Jacobs, G. A., Helber, R. W., Rowley, C., Souopgui, I., and Carrier, M. J.: Quantifying wavelengths constrained by simulated SWOT observations in a submesoscale resolving ocean analysis/forecasting system, Ocean Modelling, 135, 40–55, 2019.

De Souza, J. M. A. C., Powell, B., Castillo-Trujillo, A. C., and Flament, P.: The Vorticity Balance of the Ocean Surface in Hawaii from a Regional Reanalysis, J. Phys. Oceanogr., 45, 424–440, 2015.

Desroziers, G., Berre, L., Chapnik, B., and Poli, P.: Diagnosis of observation, background and analysis-error statistics in observation space., Quarterly Journal of the Royal Meteorological Society, 131, 3385–3396, 2005.

Di Lorenzo, E., Moore, A. M., Arango, H. G., Cornuelle, B. D., Miller, A. J., Powell, B. S., Chua, B. S., and Bennett, A. F.: Weak and Strong Constraint Data Assimilation in the inverse Regional Ocean Modelling System (ROMS): development and application for a baroclinic coastal upwelling system, Ocean Modelling, 16, 160–187, 2007.

Dibarboure, G., Anadon, C., Briol, F., Cadier, E., Chevrier, R., Delepoulle, A., Faugère, Y., Laloue, A., Morrow, R., Picot, N., et al.: Blending 2D topography images from the Surface Water and Ocean Topography (SWOT) mission into the altimeter constellation with the Level-3 multi-mission Data Unification and Altimeter Combination System (DUACS), Ocean Science, 21, 283–323, 2025.

Edwards, C. A., Moore, A. M., Hoteit, I., and Cornuelle, B. D.: Regional ocean data assimilation, Annual review of marine science, 7, 21–42, 2015.

Edwards, C. A., De Mey-Frémaux, P., Barceló-Llull, B., Charria, G., Choi, B.-J., Halliwell, G. R., Hole, L. R., Kerry, C., Kourafalou, V. H., Kurapov, A. L., et al.: Assessing impacts of observations on ocean circulation models with examples from coastal, shelf, and marginal seas, Front. Mar. Sci., 11, 1458 036, 2024.

https://doi.org/10.5194/egusphere-2026-2467
Preprint. Discussion started: 21 July 2026

Elipot, S., Lumpkin, R., Perez, R. C., Lilly, J. M., Early, J. J., and Sykulski, A. M.: A global surface drifter data set at hourly resolution, Journal of Geophysical Research: Oceans, 121, 2937–2966, 2016.

Emery, W. and Thompson, R.: Data Analysis Methods in Physical Oceanography (Second and Revised Edition), 2001.

Gille, S. T., Gao, Y., Cornuelle, B. D., and Mazloff, M. R.: SWOT Data Assimilation with Correlated Error Reduction: Fitting Model and Error Together, Journal of Atmospheric and Oceanic Technology, 2025.

Gwyther, D. E., Kerry, C., Roughan, M., and Keating, S. R.: Observing system simulation experiments reveal that subsurface temperature observations improve estimates of circulation and heat content in a dynamic western boundary current, Geoscientific Model Development, 15, 6541–6565, https://doi.org/10.5194/gmd-15-6541-2022, 2022.

Gwyther, D. E., Keating, S. R., Kerry, C., and Roughan, M.: How does 4DVar data assimilation affect the vertical representation of mesoscale eddies? A case study with observing system simulation experiments (OSSEs) using ROMS v3. 9, Geoscientific Model Development, 16, 157–178, 2023a.

Gwyther, D. E., Roughan, M., Kerry, C., and Keating, S. R.: Impact of assimilating repeated subsurface temperature transects on state estimates of a western boundary current, pp. 1–16, https://doi.org/10.3389/fmars.2022.1084784, 2023b.

Haidvogel, D. B., Arango, H. G., Hedstrom, K., Beckmann, A., Malanotte-Rizzoli, P., and Shchepetkin, A. F.: Model evaluation experiments in the North Atlantic Basin: simulations in nonlinear terrain-following coordinates, Dynam. Atmos. Oceans, 32, 239–281, 2000.

Haney, R. L.: On the Pressure Gradient Force over Steep Topography in Sigma Coordinate Ocean Models, J. Phys. Oceanogr., 21, 610–619, 1991.

Hirose, N., Takikawa, T., Ito, T., Nagamoto, A., Takagi, N., Kokubo, T., Kimura, M., Yabuki, T., and Hazama, T.: Positive data circulation established by Kyushu Smart Fisheries (QSF) team, Frontiers in Marine Science, 11, 1457 272, 2024.

Jacobs, G., D'Addezio, J. M., Ngodock, H., and Souopgui, I.: Observation and model resolution implications to ocean prediction, Ocean Modelling, 159, 101 760, 2021.

Jakoboski, J., Roughan, M., Radford, J., de Souza, J. M. A. C., Felsing, M., Smith, R., Puketapu-Waite, N., Orozco, M. M., Maxwell, K. H., and Van Vranken, C.: Partnering with the commercial fishing sector and Aotearoa New Zealand's ocean community to develop a nationwide subsurface temperature monitoring program, Progress in oceanography, 225, 103 278, 2024.

Janeković, I., Powell, B. S., Matthews, D., McManus, M. A., and Sevadjian, J.: 4D-Var Data Assimilation in a Nested, Coastal Ocean Model: A Hawaiian Case Study, J. Geophys. Res., 118, 1–14, https://doi.org/10.1002/jgrc.20389, 2013.

Kerry, C. and Roughan, M.: Downstream Evolution of the East Australian Current System: Mean Flow, Seasonal, and Intra-annual Variability, J. Geophys. Res., 125, e2019JC015 227, https://doi.org/10.1029/2019JC015227, e2019JC015227 10.1029/2019JC015227, 2020.

Kerry, C., Roughan, M., and Powell, B.: Predicting the submesoscale circulation inshore of the East Australian Current, Journal of Marine Systems, 204, 103 286, https://doi.org/https://doi.org/10.1016/j.jmarsys.2019.103286, 2020.

Kerry, C., Roughan, M., and Azevedo Correia de Souza, J. M.: Assessing the impact of subsurface temperature observations from fishing vessels on temperature and heat content estimates in shelf seas: a New Zealand case study using Observing System Simulation Experiments, Frontiers in Marine Science, 11, 1358 193, 2024a.

Kerry, C., Roughan, M., Keating, S., and Gwyther, D.: Model-based observing system evaluation in a western boundary current, Oceanography, 38, 2–12, 2025.

Kerry, C., Keating, S., Roughan, M., Azaneu, M., and Brassington, G.: Wide-swath satellite altimetry data improves modeled mesoscale and submesoscale dynamics in a western boundary current, Geophysical Research Letters, 53, e2025GL117 574, 2026a.

Kerry, C., Roughan, M., and Keating, S.: A high-resolution, 1-year, suite of 4D-Var Observing System Experiments of the East Australian Current System using the Regional Ocean Modeling System to study the impact of data from the Surface Water and Ocean Topography (SWOT) mission and Australia's Fishing Vessel Observation Network (FVON) on model state estimates, https://doi.org/10.5281/zenodo.20077064, 2026b.

Kerry, C. G. and Powell, B. S.: Including tides improves subtidal prediction in a region of strong surface and internal tides and energetic mesoscale circulation, J. Geophys. Res., 127, e2021JC018 314, 2022.

Kerry, C. G., Powell, B. S., Roughan, M., and Oke, P. R.: Development and evaluation of a high-resolution reanalysis of the East Australian Current region using the Regional Ocean Modelling System (ROMS 3.4) and Incremental Strong-Constraint 4-Dimensional Variational (IS4D-Var) data assimilation, Geosci. Model Dev., 9, 3779–3801, https://doi.org/doi:10.5194/gmd-9-3779-2016, 2016.

Kerry, C. G., Roughan, M., and Powell, B. S.: Observation Impact in a Regional Reanalysis of the East Australian Current System, J. Geophys. Res. Oceans, 123, https://doi.org/10.1029/2017JC013685, 2018.

Kerry, C. G., Roughan, M., Keating, S., Gwyther, D., Brassington, G., Siripatana, A., and Souza, J. M. A.: Comparison of 4-dimensional variational and ensemble optimal interpolation data assimilation systems using a Regional Ocean Modeling System (v3. 4) configuration of the eddy-dominated East Australian Current system, Geoscientific Model Development, 17, 2359–2386, 2024b.

Kerry, C. G., Roughan, M., Keating, S., and Brassington, G.: Wide-swath satellite altimetry and novel subsurface observations improve predictions in a dynamic western boundary current: Resolving complex fine-scale structures, Geosci. Model Dev. in prep., 2026c.

Lago, V., Roughan, M., and Caon, S.: IMOS Fishing Vessels as Ships of Opportunity (FishSOOP), Real-time Quality Assurance and Quality Control Practice Manual, Version 1.0., https://doi.org/doi.org/10.26198/sp0r-p448, 2025a.

Lago, V., Roughan, M., Kerry, C., and Knuckey, I.: Fishing for ocean data in the East Australian Current, Oceanography, 38, 67–71, https://doi.org/10.5670/oceanog.2025e105, 2025b.

Li, J., Roughan, M., and Kerry, C.: Dynamics of interannual eddy kinetic energy modulations in a western boundary current, Geophysical Research Letters, 48, https://doi.org/10.1029/2021gl094115, 2021.

Li, J., Roughan, M., and Kerry, C.: Variability and drivers of ccean temperature extremes in a warming western boundary current, Journal of Climate, 35, 1097 – 1111, https://doi.org/10.1175/JCLI-D-21-0622.1, 2022.

Liu, G., Smith, G. C., Gauthier, A.-A., Hébert-Pinard, C., Perrie, W., and Shehhi, M. R. A.: Assimilation of synthetic and real SWOT observations for the North Atlantic Ocean and Canadian east coast using the regional ice ocean prediction system, Front. Mar. Sci., 11, 1456 205, 2024.

Lorenc, A. C.: Modelling of error covariances by 4D-Var data assimilation, Quarterly Journal of the Royal Meteorological Society: A journal of the atmospheric sciences, applied meteorology and physical oceanography, 129, 3167–3182, 2003.

Lorenc, A. C. and Jardak, M.: A comparison of hybrid variational data assimilation methods for global NWP, Quarterly Journal of the Royal Meteorological Society, 144, 2748–2760, 2018.

Macdonald, H. S., Roughan, M., Baird, M. E., and Wilkin, J.: A numerical modeling study of the East Australian Current encircling and overwashing a warm-core eddy, J. Geophys. Res., 118, 301–315, https://doi.org/10.1029/2012JC008386, 2013.

Malan, N., Roughan, M., and Kerry, C.: The rate of coastal temperature rise adjacent to a warming western boundary current is nonuniform with latitude, Geophysical Research Letters, 48, e2020GL090 751, https://doi.org/10.1029/2020GL090751, 2021.

Malan, N., Roughan, M., Hemming, M., and Schaeffer, A.: Mesoscale Circulation Controls Chlorophyll Concentrations in the East Australian Current Separation Zone, J. Geophys. Res., 128, e2022JC019 361, 2023.

Martin, M. J., Hoteit, I., Bertino, L., and Moore, A. M.: Data assimilation schemes for ocean forecasting: state of the art, State of the Planet Discussions, 2024, 1–16, 2024.

Matisons, L., Moninya, R., Amandine, S., and Colette, K.: SWOT Assimilation Improves Lagrangian Trajectory and Mesoscale Eddy Representation in a Dynamic Western Boundary Current, Geophysical Research Letters, In prep., 2026.

Matthews, D., Powell, B. S., and Janekovic, I.: Analysis of four-dimensional variational state estimation of the Hawaiian waters, J. Geophys. Res., 117, 2012a.

Matthews, D., Powell, B. S., and Janeković, I.: Analysis of Four-dimensional Variational State Estimation of the Hawaiian Waters, J. Geophys. Res., 117, https://doi.org/10.1029/2011JC007575, 2012b.

Mellor, G. L., Ezer, T., and Oey, L. Y.: The pressure gradient error conundrum of sigma coordinate ocean models, J. Atmos. Ocean. Technol., 11, 1126–1134, 1994.

Moore, A., Martin, M., Akella, S., Arango, H., Balmaseda, M., Bertino, L., Ciavatta, S., Cornuelle, B., Cummings, J., Frolov, S., Lermusiaux, P., Oddo, P., Oke, P., Storto, A., Teruzzi, A., Vidard, A., and Weaver, A.: Synthesis of Ocean Observations Using Data Assimilation for Operational, Real-Time and Reanalysis Systems: A More Complete Picture of the State of the Ocean, Front. Mar. Sci., 6, 90, https://doi.org/10.3389/fmars.2019.00090, 2019.

Moore, A., Zavala-Garay, J., Arango, H. G., Edwards, C. A., Anderson, J., and Hoar, T.: Regional and basin scale applications of ensemble adjustment Kalman filter and 4D-Var ocean data assimilation systems, Prog. Oceanogr., 189, 102 450, 2020.

Moore, A. M., Arango, H. G., Di Lorenzo, E., Cornuelle, B. D., Miller, A. J., and Neilson, D. J.: A comprehensive ocean prediction and analysis system based on the tangent linear and adjoint of a regional ocean model, Ocean Modelling, 7, 227–258, 2004.

Moore, A. M., Arango, H. G., Broquet, G., Edwards, C., Veneziani, M., Powell, B. S., Foley, D., Doyle, J., Costa, D., and Robinson, P.: The Regional Ocean Modeling System (ROMS) 4-dimensional variational data assimilation systems: Part II – Performance and application to the California Current System, Prog. Oceanog., 91, 50–73, https://doi.org/10.1016/j.pocean.2011.05.003, 2011a.

Moore, A. M., Arango, H. G., Broquet, G., Edwards, C., Veneziani, M., Powell, B. S., Foley, D., Doyle, J., Costa, D., and Robinson, P.: The Regional Ocean Modeling System (ROMS) 4-dimensional variational data assimilation systems: Part III – Observation impact and observation sensitivity in the California Current System, Prog. Oceanog., 91, 74–94, https://doi.org/10.1016/j.pocean.2011.05.005, 2011b.

Moore, A. M., Arango, H. G., Broquet, G., Powell, B. S., Zavala-Garay, J., and Weaver, A. T.: The Regional Ocean Modeling System (ROMS) 4-dimensional variational data assimilation systems: Part I – System overview and formulation, Prog. Oceanog., 91, 34–49, https://doi.org/10.1016/j.pocean.2011.05.004, 2011c.

Morrow, R., Fu, L.-L., Ardhuin, F., Benkiran, M., Chapron, B., Cosme, E., d'Ovidio, F., Farrar, J. T., Gille, S. T., Lapeyre, G., et al.: Global observations of fine-scale ocean surface topography with the surface water and ocean topography (SWOT) mission, Front. Mar. Sci., 6, 232, 2019.

Oke, P. R. and Griffin, D. A.: The cold-core eddy and strong upwelling off the coast of New South Wales in early 2007, Deep Sea Research Part II: Topical Studies in Oceanography, 58, 574 – 591, https://doi.org/https://doi.org/10.1016/j.dsr2.2010.06.006, the East Australian Current – Its Eddies and Impacts, 2011.

Oke, P. R. and Sakov, P.: Representation error of oceanic observations for data assimilation, Journal of Atmospheric and Oceanic Technology, 25, 1004–1017, 2008.

Oke, P. R., Roughan, M., Cetina-Heredia, P., Pilo, G. S., Ridgway, K. R., Rykova, T., Archer, M. R., Coleman, R. C., Kerry, C. G., Rocha, C., Schaeffer, A., and Vitarelli, E.: Revisiting the circulation of the East Australian Current: its path, separation, and eddy field, Prog. Oceanogr., 176, 2019.

https://doi.org/10.5194/egusphere-2026-2467
Preprint. Discussion started: 21 July 2026

Pasmans, I., Kurapov, A. L., Barth, J. A., Ignatov, A., Kosro, P. M., and Shearman, R. K.: Why Gliders Appreciate Good Company: Glider Assimilation in the Oregon-Washington Coastal Ocean 4DVAR System With and Without Surface Observations, J. Geophys. Res., 124, 750–772, https://doi.org/10.1029/2018JC014230, 2019.

Pilo, G. S., Mata, M. M., and Azevedo, J. d.: Eddy surface properties and propagation at Southern Hemisphere western boundary current systems, Ocean Science, 11, 629–641, 2015a.

Pilo, G. S., Oke, P. R., Rykova, T., Coleman, R., and Ridgway, K.: Do East Australian Current anticyclonic eddies leave the Tasman Sea?, J. Geophys. Res., 120, 8099–8114, 2015b.

Pilo, G. S., Oke, P. R., Coleman, R., Rykova, T., and Ridgway, K.: Patterns of vertical velocity induced by eddy distortion in an ocean model, J. Geophys. Res., 123, 2274–2292, 2018.

Powell, B. S. and Moore, A. M.: Estimating the 4DVAR analysis error of GODAE products, Ocean Dynamics, 59, 121–138, 2008.

Powell, B. S., Arango, H. G., Moore, A. M., Di Lorenzo, E., Milliff, R. F., and Foley, D.: 4DVAR data assimilation in the Intra-Americas Sea with the Regional Ocean Modeling System (ROMS), Ocean Modell., 25, 173–188, 2008.

Pujol, M.-I., Faugère, Y., Taburet, G., Dupuy, S., Pelloquin, C., Ablain, M., and Picot, N.: DUACS DT2014: the new multi-mission altimeter data set reprocessed over 20 years, Ocean Science, 12, 1067–1090, 2016.

Raynaud, L., Berre, L., and Desroziers, G.: An extended specification of flow-dependent background error variances in the Météo-France global 4D-Var system, Quarterly Journal of the Royal Meteorological Society, 137, 607–619, 2011.

Roughan, M. and Kerry, C.: South East Australian Coastal Ocean Forecast System (SEA-COFS), https://doi.org/10.5281/zenodo.8294716, We acknowledge funding from the Australian Research Council including grants: DP230100505, LP220100515, LP170100498, LP160100162, LP150100064, DP140102337, LP120100592, 2023.

Roughan, M., Macdonald, H. S., Baird, M. E., and Glasby, T. M.: Modelling coastal connectivity in a Western Boundary Current: Seasonal and inter-annual variability, Deep Sea Research Part II: Topical Studies in Oceanography, 58, 628–644, 2011.

Roughan, M., Keating, S., Schaeffer, A., Cetina Heredia, P., Rocha, C., Griffin, D., Robertson, R., and Suthers, I.: A tale of two eddies: The biophysical characteristics of two contrasting cyclonic eddies in the e ast a ustralian c urrent s ystem, J. Geophys. Res., 122, 2494–2518, 2017.

Rykova, T. and Oke, P. R.: Stacking of EAC eddies observed from Argo, J. Geophys. Res., 127, e2022JC018 679, 2022.

Schaeffer, A. and Roughan, M.: Influence of a western boundary current on shelf dynamics and upwelling from repeat glider deployments, Geophysical Research Letters, 42, 121–128, 2015.

Schaeffer, A., Roughan, M., and Wood, J. E.: Observed bottom boundary layer transport and uplift on the continental shelf adjacent to a western boundary current, J. Geophys. Res. Oceans, 119, 1–18, 2014.

Schaeffer, A., Roughan, M., Jones, E., and White, D.: Physical and biogeochemical spatial scales of variability in the East Australian Current separation zone from shelf glider measurements, Biogeosciences Discuss., 13, 1967–1975, 2015.

Shchepetkin, A. F. and McWilliams, J. C.: The regional oceanic modeling system (ROMS): a split-explicit, free-surface, topography-following-coordinate oceanic model, Ocean Modell., 9, 347–404, 2005.

Siripatana, A., Kerry, C., Roughan, M., Souza, J. M. A., and Keating, S.: Assessing the impact of nontraditional ocean observations for prediction of the East Australian Current, J. Geophys. Res., 125, e2020JC016 580, 2020.

Sloyan, B. M., Ridgway, K. R., and Cowley, R.: The East Australian Current and Property Transport at 27S from 2012-2013., J. Phys. Oceanogr., 46, 2016.

Souza, J., Powell, B. S., Castillo-Trujillo, A. C., and Flament, P.: The Vorticity Balance of the Ocean Surface in Hawaii from a Regional Reanalysis, J. Phys. Oceanogr., 45, 424–440, 2014.

Tamtare, T., Dumont, D., and Chavanne, C.: The Stokes drift in ocean surface drift prediction, Journal of Operational Oceanography, 15, 156–168, 2022.

Tchonang, B. C., Benkiran, M., Le Traon, P.-Y., Jan van Gennip, S., Lellouche, J. M., and Ruggiero, G.: Assessing the impact of the assimilation of SWOT observations in a global high-resolution analysis and forecasting system–part 2: results, Front. Mar. Sci., 8, 687 414, 2021.

Tranchant, Y.-T., Legresy, B., Foppert, A., Pena-Molino, B., and Phillips, H.: SWOT reveals fine-scale balanced motions driving near-surface currents and dispersion in the Antarctic Circumpolar Current, Earth and Space Science, 12, e2025EA004 248, 2025.

Tréboutte, A., Carli, E., Ballarotta, M., Carpentier, B., Faugère, Y., and Dibarboure, G.: KaRIn noise reduction using a convolutional neural network for the SWOT ocean products, Remote Sensing, 15, 2183, 2023.

Vranken, C. V., Jakoboski, J., Carroll, J. W., Cusack, C., Gorringe, P., Hirose, N., Manning, J., Martinelli, M., Penna, P., Pickering, M., Piecho-Santos, A. M., Roughan, M., et al.: Towards a global Fishing Vessel Ocean Observing Network (FVON): state of the art and future directions, Frontiers in Marine Science, 10, 1176 814, https://doi.org/https://doi.org/10.3389/fmars.2023.1176814, 2023.

Walstad, L. J. and McGillicuddy, D. J.: Data assimilation for coastal observing systems, Oceanography, 13, 47–53, 2000.

Weaver, A. and Courtier, P.: Correlation modelling on the sphere using generalized diffusion equation., Quart. J. Roy. Meteorol. Soc., 127, 1815–1846, 2001.

Wilkin, J., Levin, J., Moore, A., Arango, H., López, A., and Hunter, E.: A data-assimilative model reanalysis of the US Mid Atlantic Bight and Gulf of Maine: Configuration and comparison to observations and global ocean models, Prog. Oceanogr., 209, 102 919, 2022.

Zavala-Garay, J., Wilkin, J. L., and Arango, H. G.: Predictability of mesoscale variability in the East Australian Current given strong-constraint data assimilation, J. Phys. Oceanogr., 42, 1402–1420, 2012.